Construction and Building Materials 333 (2022) 127386

Contents lists available at ScienceDirect

Construction and Building Materials

journal homepage: www.elsevier.com/locate/conbuildmat

Hydration kinetics and phase evolution of Portland cement composites containing sodium-montmorillonite functionalized with a Non-Ionic surfactant

Dayou Luo, Jianqiang Wei *

Department of Civil and Environmental Engineering, Francis College of Engineering, University of Massachusetts Lowell, Lowell, MA 01854, USA

ARTICLE INFO

Keywords:
Cement composite
Hydration kinetics
Montmorillonite
Functionalization
Non-ionic surfactant
Dispersion
Dynamic moisture sorption
Mechanical properties
Microstructure

ABSTRACT

This study investigates the hydration behavior and phase evolution of portland cement composites containing montmorillonite (MT) with an objective to address the poor dispersion and improve physical features and chemical reactivity of MT through functionalization with a non-ionic surfactant (polyethylene glycol ether). After functionalization, the MT exhibited an enlarged layer spacing (122%), organic chemical bonds intercalated, improved dispersion in concrete pore solutions, reduced moisture sorption capacity. The cement composites containing the functionalized MT showed enhanced cement hydration, less portlandite, more calcium silicate hydrates (C-S-H) and aluminum-containing hydrates, a more densified microstructure, and higher strength than the composites with raw MT.

1. Introduction

Cement is the most widely used artificial material with an annual average production of more than 4 billion tons globally [1], which is still significantly increasing due to urbanization and industrial development. Partially replacing cement with supplementary cementitious materials (SCMs), such as fly ash, metakaolin, montmorillonite (MT), granulated blast furnace slag, silica fume, ground waste glass, etc. [2–6], has been proven a promising and practical approach to decrease cement usage and modify cement hydration, improve properties and prolong the service life of concrete structures. Among these SCMs, clay-based natural pozzolans that are abundant, widely available, easy to proceed with unique physical properties, and high pozzolanic reactivity are attracting increasing attention in developing higher performance cementitious composites.

MT, the main and active constituent of bentonite, is a widely distributed and worldwide abundant natural clay mineral with a 2:1 layered structure consisting of two stacked tetrahedral silicate sheets and an octahedral aluminate sheet. The Si^{4+} in tetrahedral sheets is partially substituted by Al^{3+}, resulting in an overall negative charge counterbalanced by some exchangeable cations (i.e., sodium, potassium, calcium, magnesium) in the interlayer spaces [7]. It is believed that ions or some big molecules could intercalate into the interlayer space of sMT by diffusion to replace the district cations and induce swelling or collapse of the clay structure [8]. MT is highly hydrophilic as the water molecules could easily interleave in its interlayer space and be absorbed by the hydrated cations, thereby presenting an excellent water swelling property [9]. Especially noteworthy is the higher water uptake capacity of the monovalent cations (sodium) than the divalent ones (calcium and magnesium). Moreover, MT possesses an extraordinary pozzolanic reactivity due to the high contents of reactive aluminate and silica [10]. Extensive investigations have been performed to support that the cement hydration could be enhanced in the presence of MT either by the filler effect or the pozzolanic reaction, thereby densifying the microstructure, improving the mechanical strength, and increasing the durability of the cement composites [2,11]. However, when using MT as an SCM for cement substitution, detrimental effects and limitations have been identified: (i) the optimal dosage of MT in improving the mechanical strength was reported at a cement replacement level between 1% and 3% by mass [12], and (ii) the high agglomeration of MT due to the van der Waals force and electrostatic force among MT nanosheets in the presence of water might result in poor dispersion and negatively impact its pozzolanic reactivity in the matrix of cement as well as the performance of the concrete [10,13,14].

* Corresponding author.
E-mail address: Jianqiang_Wei@uml.edu (J. Wei).

https://doi.org/10.1016/j.conbuildmat.2022.127386
Received 9 December 2021; Received in revised form 29 March 2022; Accepted 2 April 2022
Available online 8 April 2022

With an objective to address the agglomeration and dispersion issues of MT in cement composites, extensive investigations have been conducted, and they can be categorized into two approaches: physical method and chemical method. The physical approaches involve the use of electric mixers [15], high-shear mixers [16], ultrasonic homogenizers [17], etc. The chemical approaches are primarily focusing on functionalization with various surfactants by leveraging the unique layered structure of MT. The most used cationic surfactants are mainly quaternary ammonium salts, such astetramethylammonium bromide, decyltrimethylammonium bromide, hexadecyltrimethylammonium bromide [18], methyl-benzyl-dihydrogenated tallow ammonium chloride, dimethyl-benzyl-hydrogenated tallow ammonium chloride, dimethyl-dihydrogenated tallow ammonium chloride [19], octadecyltrimethyl ammonium bromide, dioctadecyl dimethylammonium bromide [20], and cethyl trimethyl ammonium bromide [21], which can increase the dispersion of the clay particles in the cement matrix, densify the microstructure of hydrated cement, and improve the mechanical properties of cement composites. Other cationic surfactants, such as trihexyl tetradecyl phosphonium chloride [22], and *n*-alkyl 4-pyridinecarboxylate [23], were also used for functionalizing sMT. Since the microstructure of cement pastes can be influenced by the interlayer spacing of the functionalized sMT, the alkyl chain length, and the type of surfactants, the surfactants for functionalizing sMT should be well-selected and designed [18,19]. Although enhanced hydration and improved properties can be obtained by incorporating functionalized MT, it was found that the optimal cement replacement for seeking both strength and durability improvement is still less than 1% [21,24–26]. At higher cement substitution levels, a decreased strength would be induced. Moreover, the toxicity of cationic surfactants [22] has driven new investigations on non-ionic surfactants with less toxic characteristics [27]. Guégan [28] functionalized sMT with triethylene glycol mono-*n*-decyl ether, which presented a bilayer structure within the interlayer space of sMT. Papatzani and Paine [29] observed that the non-ionic fatty alcohol increased the dispersion of sMT in cement composite, but its dispersion is somewhat unstable.

The present paper investigated the effect of the organic sMT functionalized by a non-ionic surfactant PEG10 on the hydration kinetics and property development of cement composites. The amount of intercalated surfactants, crystallinity, interlayer spacing, chemical bonds, dispersion of MT particles in concrete pore solutions, moisture and water absorption of the functionalized sMT were characterized with thermogravimetric analysis (TGA), X-ray diffraction (XRD), attenuated total reflection-Fourier transforms infrared spectroscopy (ATR-FTIR), ultraviolet–visible spectrophotometry (UV–Vis) and dynamic vapor sorption (DVS). To obtain a comprehensive understanding of cement hydration kinetics, hydration products, microstructure, and property development of cement composites containing the functionalized MT, isothermal calorimetry, TGA, XRD, ATR-FTIR, Raman spectroscopy, compressive strength test, and field emission scanning electron microscopy (FE-SEM) were performed.

2. Materials and methods

2.1. Materials

The cementitious materials used were Type I/II ordinary Portland cement (ASTM C150 [30]) produced by Quikrete and sodium-montmorillonite (sMT) in powder form (Sigma-Aldrich) with a relative density of 2.4 g/cm^3 and a molecular weight of 180.1 g/mol. The chemical and mineralogical compositions of the cement and sMT, analyzed by X-ray fluoresce (XRF) and Bogue calculation, are summarized in Table 1. It shows that the silicate and aluminate phases (SiO_2 + Al_2O_3) in sMT are higher than 79 wt% with contents of Na_2O, Fe_2O_3, and MgO of 5.03%, 6.51%, and 7.356%, respectively. The particle size distributions (PSD) of cement and sMT measured by laser diffraction are shown in Fig. 1. The cement has a specific surface area and median particle size of 1.66 m^2/g and 12.2 μm, respectively, while the sMT exhibits finer particles with a specific surface area of 0.86 m^2/g and a median particle size of 7.9 μm. The cation exchange capacity (CEC) of sMT is 116.48 meq/100 g, which was determined by Methylene blue test according to ASTM C837 [31]. A chemically pure non-ionic surfactant, polyethylene glycol ether (PEG10, purchased from Sigma-Aldrich) with an average molar mass of 660 g/mol, was used to functionalize the sMT organically.

Table 1
Chemical and mineralogical compositions of the cementing materials.

Oxide composition [wt.%]			Mineralogical phase composition of cement [wt.%]	
	sMT	Cement		
CaO	0.949	62.7	Tricalcium silicate (C_3S)	54
SiO_2	62.0	20.1		
Al_2O_3	17.2	4.8		
SO_3	0.199	3.5	Dicalcium silicate (C_2S)	17
Fe_2O_3	6.51	3.2		
MgO	7.35	3.4		
SrO	0.0442	–	Tricalcium aluminate (C_3A)	7
K_2O	0.0717	Na_2O +		
Na_2O	5.03	0.658K_2O		
		0.60		
TiO_2	0.224	–	Tetra-calcium aluminoferrite	10
ZnO	0.0283	–	(C_4AF)	
ZrO_2	0.146	–		
Cl	0.185	–	Limestone	1.2
Compton	0.86	–		
Rayleigh	1.03	–		

By leveraging the layered structure with exchangeable cations (Na^+, Ca^{2+}) in the interlayer space, montmorillonite (MT) could be organically functionalized by surfactant through an ion-exchange method [32] controlled by nanoscale chemical–mechanical coupling [8]. In this study, sMT was mixed with PEG10 in deionized water at 500 rpm for 30 min at 25 °C as detailed in the author's previous work [33] to obtain functionalized organic sMT. The concentration of PEG10 was equivalent to 0.2 CEC of sMT, and the functionalized clay was expressed as PEG10-sMT. Reagent grade calcium hydroxide (97%), sodium metasilicate (≥97%), sodium aluminate (99.9%), potassium hydroxide (97%), potassium sulfate (99.2%), and sodium hydroxide (≥85%) were used for simulating concrete pore solutions.

2.2. Mixture proportions and sample preparation

As summarized in Table 2, in this study, the water to binder (w/b) ratio for all the cement blends was fixed at 0.40. The reference group was prepared by mixing neat Portland cement with water and noted as PC. It has been reported that the optimum dosage of MT as a cement substitute to improve hydration and mechanical properties is between 1% and 5% [24,34,35]. Two groups with 1 wt% and 3 wt% cement replacements with raw sMT were named sMT-1 and sMT-2, respectively. Correspondingly, two cement blends incorporated with 1 wt% and 3 wt % of PEG10-sMT (PEG10-sMT-1 and PEG10-sMT-3) were also prepared to explore the role of the organic sMT functionalized with PEG-10 in cement hydration. By taking the weight of surfactant into account, the mass of the functionalized sMT in PEG10-sMT-1 and PEG10-sMT-3 was normalized by the mass fraction of sMT to ensure that the binary cement blends with raw and functionalized sMT have the same amount of sMT at each cement substitution level (see Table 2).

Fresh cement pastes for TGA, XRD, ATR-FTIR spectroscopy and SEM investigations were mixed in a vacuum mixer at 500 rpm for 3 min to obtain homogenous mixtures and avoid air bubbles. Subsequently, the pastes were sealed in plastic containers, which were then stored at 23 ± 2 °C in a vacuum desiccator with soda lime to avoid carbonation. At each testing age, the paste samples were ground into fine powders, and then the cement hydration was stopped by solvent exchanging with alcohol for 24 h. For compressive strength investigations, mortar samples were prepared based on the cement binders according to the proportion

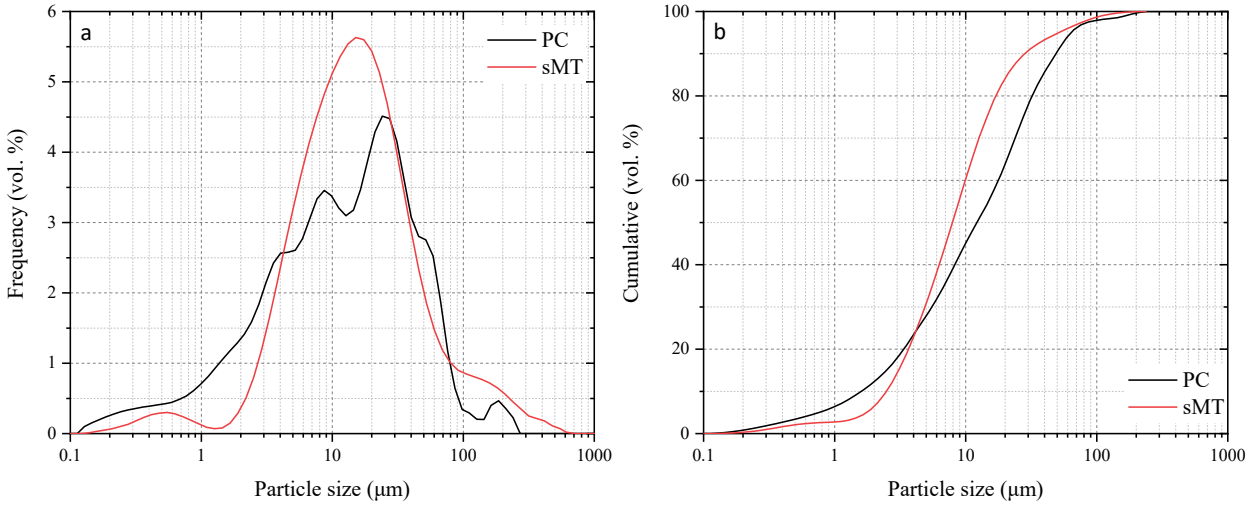

Fig. 1. Particle size distributions of the cement and sMT: (a) the relative frequency of particles based on diameter, (b) volume of the particles smaller than a specific diameter.

Table 2
Compositions of cement mixtures.

Index	Content (g)				W/b
	Cement	Water	sMT	Sand	
PC	100	40	–	100	0.40
sMT-1	99	40	1	100	0.40
sMT-3	97	40	3	100	0.40
PEG10-sMT-1	99	40	1	100	0.40
PEG10-sMT-3	97	40	3	100	0.40

design summarized in Table 2. A w/b ratio of 0.4 and a binder-to-sand ratio of 1.0 were employed for all the five mortar mixtures. The cement pastes were mixed with gradually added sand in a mechanical mortar mixer at 60 rpm for 2 min, followed by a 1-minute rest and another 3 min of faster mixing at 120 rpm. Then, three 50 mm by 50 mm by 50 mm cubic samples were cast for each testing age per ASTM C109/109 M [36]. Right after casting, the specimens and molds were covered with a plastic sheet to avoid water loss. The specimens were demolded after 24 h and cured in saturated CH solution at 23 ± 2 °C until testing.

2.3. Experimental methods

Isothermal calorimetry was performed with an I-Cal 2000 HPC high precision isothermal calorimeter to measure the heat flow and cumulative heat release of the cement pastes during the first 50 h of hydration at 25 °C. For each measurement, the raw materials, i.e., cement, sMT, or PEG10-sMT, and mixing water, were conditioned in the calorimeter chambers at the target temperature for 24 h. 50 g pastes with a w/b ratio of 0.40 were mixed homogeneously by hand at a temperature of 25 ± 2 °C. Within 1 min after the initial water-cement contact, the well-mixed paste samples were sealed in plastic containers and placed in the calorimeter chambers to record the heat of hydration.

TGA was carried out on clay (sMT and PEG10-sMT) and ground powders of the cement pastes after 7, 28, and 90 days using a Perkin Elmer TGA 4000 thermogravimetric analyzer. For each test, a 20–40 mg powder sample was maintained at 30 °C for 3 min, followed by a temperature increase from 30 °C to 800 °C at a heating rate of 15 °C/min under N_2 purge gas at a flow rate of 20 mL/min. The contents of CH and $CaCO_3$ (CC) in the cement pastes, corresponding to the weight loss between 400 °C and 570 °C and the weight loss between 590 °C and 770 °C, respectively, were determined by using the following equations:

$$CH_1 = \left[\frac{W_{400} - W_{510}}{W_{510}}\right] \times \frac{M_{CH}}{M_{H_2O}} = \left[\frac{W_{400} - W_{570}}{W_{510}}\right] \times 4.1 \times 100\% \quad (1)$$

$$CC = \left[\frac{W_{590} - W_{770}}{W_{770}}\right] \times \frac{M_{CC}}{M_{CO_2}} = \left[\frac{W_{590} - W_{770}}{W_{770}}\right] \times 2.27 \times 100\% \quad (2)$$

where W_n is the mass at temperature n °C. Note that the temperature boundaries of CH and CC might slightly vary for each sample, i.e., the temperatures are not fixed at the values shown in Eq. (1) and Eq. (2). Instead, the temperature ranges were determined on the TGA and DTG curves via a tangent method [37]. M_{CH}, M_{H2O}, M_{CC}, and M_{CO2} are the molar mass of CH, H_2O, CC, and CO_2, respectively. CC is mainly due to the slight carbonation of CH in the pastes during the process of sample preparation. Thus, in this study, the total CH content was calculated by summing the CH in Eq. (1), and the CH_2 converted from CC, and then subtracting the mass of limestone (LS, 1.2% as listed in Table 1) originally contained in the Portland cement as follows:

$$CH_2 = (CC - f_C \bullet LS) \times \frac{M_{CH}}{M_{CC}} = CC \times 0.74 \quad (3)$$

$$CH = CH_1 + CH_2 \quad (4)$$

where f_C is the mass fraction of cement in the blends.

Generally, the evaporable water is expected to be removed between the temperature range of 30–115 °C. The decomposition of the cement hydration products shown as the endothermic peaks on the DTG curves could be divided into three stages: dehydration, dehydroxylation, and decarbonization [38]. The first stage between 120 and 400 °C was due to the weight loss of the chemically bound water in water-rich phases, such as C-S-H, ettringite (AFt), strätlingite, calcium monosulfoaluminate (AFm), etc. The dehydroxylation of CH is within the temperature range of 400–570 °C, while the third phase within the temperature range of 570–800 °C was corresponding to the decarbonization of CC. Thus, the content of chemically bound water (W_B) was calculated as follows by summing the water loss from TGA curves in the dehydration, dihydroxylation, and the one converted from the mass loss due to the decarbonization of CC by multiplying the molar mass ratio of water and carbon dioxide (0.41):

$$W_B = Ldh + Ldx + 0.41Ldc \quad (5)$$

where *Ldh*, *Ldx*, *and Ldc* represent the mass loss on TGA curves during dehydration of cement hydrates (i.e., C-S-H, ettringite, and AFm), dehydroxylation of CH, and decarbonization of CC (excluding the

limestone contained in Portland cement), respectively. Although CC (excluding the original limestone content in cement) does not contain water, this phase is converted from CH due to carbonation. In an ideal condition, where the carbonation can be fully mitigated, there should not be the formation of the extra CC, and the CH can remain in the system. To obtain an accurate evaluation of chemically bound water, the entire hydration process was covered. Therefore, the carbonated CH (i.e., CC) was included in the calculation of chemically bound water.

The method proposed by Bhatty [39] was modified to calculate the degree of cement hydration (*DOH*) by normalizing W_B by the mass fraction of cement in the blends (f_c) and the ultimate chemically bound water per gram of fully hydrated cement (0.25 g/g) [40,41].

$$DOH = \frac{W_B}{0.25 \bullet f_c} \tag{6}$$

XRD investigation was performed on clay and ground cement powders after 7, 28, and 90 days of hydration using an AXRD powder X-ray diffractometer equipped with a CuKα source ($\lambda = 1.54$ Å) at 30 kV and 20 mA. The samples were scanned on a rotary support in stepwise mode from 15° to 65° with a step size of 0.02° (2θ) and a scanning time of 5 s per step. The obtained XRD data was analyzed using XRDWIN®PD software combined with the Crystallography Open Database (COD) [42]. The basal space of the clay particles was determined from the XRD data based on the Bragg equation (Eq. (7)) [43]:

$$d = \frac{n\lambda}{2\sin\theta} \tag{7}$$

where d, θ, n and λ are basal spacing, angles of incidence, diffraction order, and X-ray wavelength, respectively.

The moisture absorption and desorption behavior of both raw and functionalized sMT were characterized at 25 °C via dynamic vapor sorption (DVS) analysis using a DVS INTRINSIC II system (Surface Measurement System LTD, PA). The mass changes of about 20 mg samples at varying relative humidity (RH) controlled by the modulation between flows of dry N_2 and HPLC grade water vapor were monitored. The absorption behavior was tested starting with an initial RH of 0, then increased to 90% with a 10% increment, followed by a 5% increment up to 95% RH. The desorption process was measured through reversed humidity steps from 95% to 90%, followed by a 10% RH decrement to 0. For each RH step, equilibrium was considered to be reached when the mass change rate is less than 0.002% per minute over 5 min, from where sorption isotherms were determined by plotting equilibrium mass as a function of RH.

The dispersion of sMT and PEG10-sMT in a simulated concrete pore solution was evaluated by UV–Vis spectroscopy in a wavelength range of 200–1000 nm using a Cary 8454 spectrophotometer with a scanning interval of 1 nm. The simulated concrete pore solution was prepared by mixing reagent grade calcium nitrate, sodium metasilicate, sodium aluminate, potassium hydroxide, potassium sulfate, and sodium hydroxide in deionized water. Based on the real pore solution extracted from cement paste at 69 days according to [44], the simulated concrete pore solution was synthesized with the elemental concentrations of K, Na, Ca, Si, and Al as 493.63 mM, 44.93 mM, 2.44 mM, 0.15 mM, and 0.09 mM, respectively. Approximately 1 mg/mL of clay particles (less than 40 μm) were dispersed in the simulated concrete pore solution in an ultrasonic bath and ultrasonicated for 15 min before measuring.

The microstructure of selected cement pastes after 90 days of hydration was investigated on polished surfaces using a JEOL JSM 7401F FE-SEM under an accelerating voltage of 10.0 kV. The main hydration products, such as C-S-H, ettringite, portlandite (CH), were morphologically characterized.

ATR-FTIR spectroscopy was performed on cement paste powders after 7, 28, and 90 days using a Thermo Fisher Scientific Nicolet iS10 FTIR spectrometer. The ATR-FTIR signals were acquired by pressing the powders to the ATR diamond to interact with the IR light. The spectra between 4000 and 400 cm^{-1} were acquired by the co-addition of 32 scans with a resolution of 4 cm^{-1}.

Raman spectroscopy was conducted on cement pastes powders after 7 and 90 days of hydration using a Horiba LabRam HR Evolution Raman Spectrometer over the range of 200 cm^{-1} to 1700 cm^{-1}. A 532 nm excitation laser with a maximum power of 2.8 mW was utilized under a 50 × objective lens with an acquisition time of 60 s. 2 accumulations were collected for each sample. The as-received data was processed with LabSpec 6 Spectroscopy Suite by removing the background and fitting the peaks with the Gaussian function.

The development of compressive strength of the mortar mixtures was monitored on cubic mortar specimens according to ASTM C109 (2021) [36]. Three repetitions of mortar cubes for each group, after being cured in a saturated CH solution for 1, 7, 28, and 90 days, were tested using a CONTROLS automatic concrete compression machine at a loading rate of 900 N/s. The peak load yielded by the samples was used for determining the compressive strength by averaging the three repetitions.

3. Results and discussion

3.1. Characterization of sMT

3.1.1. TGA

The TGA of the sMT and PEG10-sMT is shown in Fig. 2. It can be seen from Fig. 2a and 2b that a new endothermic peak in the temperature range of 270 to 540 °C could be identified from the PEG10-sMT, which was attributed to the thermal decomposition of the surfactant. From the corresponding weight loss in the TGA curve, it was found that 11.5% of PEG10-sMT was occupied by the surfactant. The weight losses before 200 °C and after 540 °C in both curves were attributed to the evaporations of surface and interlayer water and the decomposition of sMT particles, respectively. The weight losses of 11.8% and 4.5% due to the water evaporation of sMT and PEG10-sMT were observed, respectively, while the values due to the decomposition of sMT particles were 3.7% and 3.2%.

3.1.2. XRD and FTIR

As illustrated in XRD patterns (Fig. 3a), due to the intercalation of PEG10, the basal space of sMT was increased from 1.52 nm (5.80° 2θ) to 1.85 nm (4.78° 2θ). A new peak corresponding to 0.53 nm was also observed from the PEG10-sMT. The divergences in ATR-FTIR spectra of sMT and PEG10-sMT in Fig. 3b confirmed the intercalation of PEG10 into sMT by two distinguishable regions of 3025–2800 cm^{-1} and 1535–1175 cm^{-1}. The former spectral band was caused by the symmetric and asymmetric stretching and bending vibrations of aliphatic chains (–CH_2/–CH_3) from PEG10. In the latter region, the peaks appearing at ~ 1353 cm^{-1} and ~ 1295 cm^{-1} are due to the methylene deformation mode and the C-O group attached with a methyl group, respectively. The benzene ring skeleton in surfactants can be observed from the spectra at ~ 1512 cm^{-1} and ~ 1459 cm^{-1}.

3.1.3. Moisture absorption and desorption behavior

The mass change of sMT and PEG10-sMT, normalized by the fraction of raw sMT, as a function of time under varying RH and the corresponding isotherms are shown in Fig. 4a and 4b, respectively. From the vapor sorption profiles (Fig. 4a), it can be seen that the mass of PEG10-sMT reached equilibrium in both adsorption and desorption faster than sMT. The sMT took around 50.5 h to complete an "adsorption–desorption" cycle, while PEG10-sMT was completed with 10 fewer hours. Although the interlayer space was enlarged, at each of the increased and decreased RH steps, the sMT showed lower equilibrium mass after functionalization. At 95% RH, the equilibrium mass gain of sMT is 36.0%, which is 8.5% higher than that of PEG10-sMT. As shown in Fig. 4b, the sorption isotherms of sMT and PEG10-sMT share the same path in line with the type II pattern according to the classification proposed by the International Union of Pure and Applied Chemists (IUPAC) [45]. Three segments can be identified from these sorption isotherms

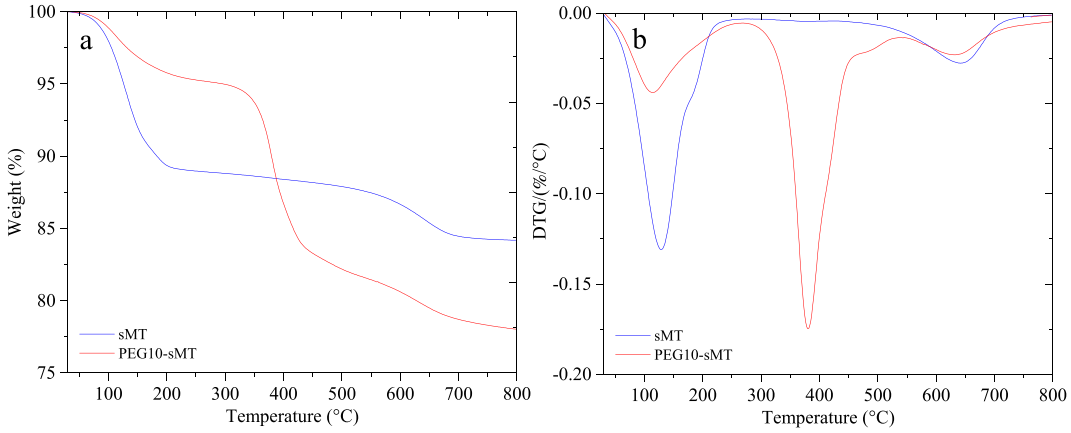

Fig. 2. (a) TGA and (b) DTG curves of sMT and PEG10-sMT.

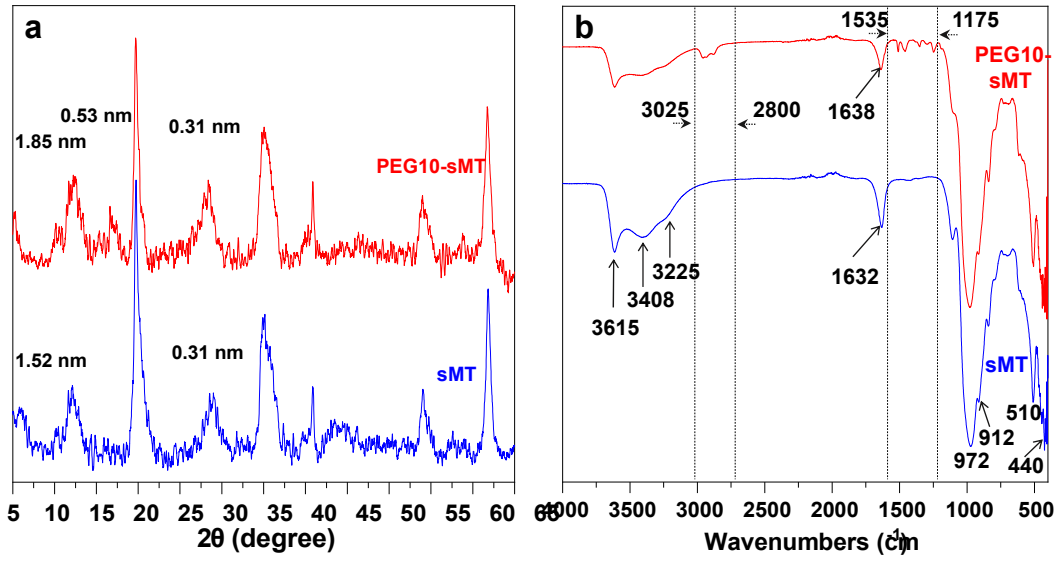

Fig. 3. (a) XRD patterns and (b) ATR-FTIR spectra of sMT and PEG10-sMT.

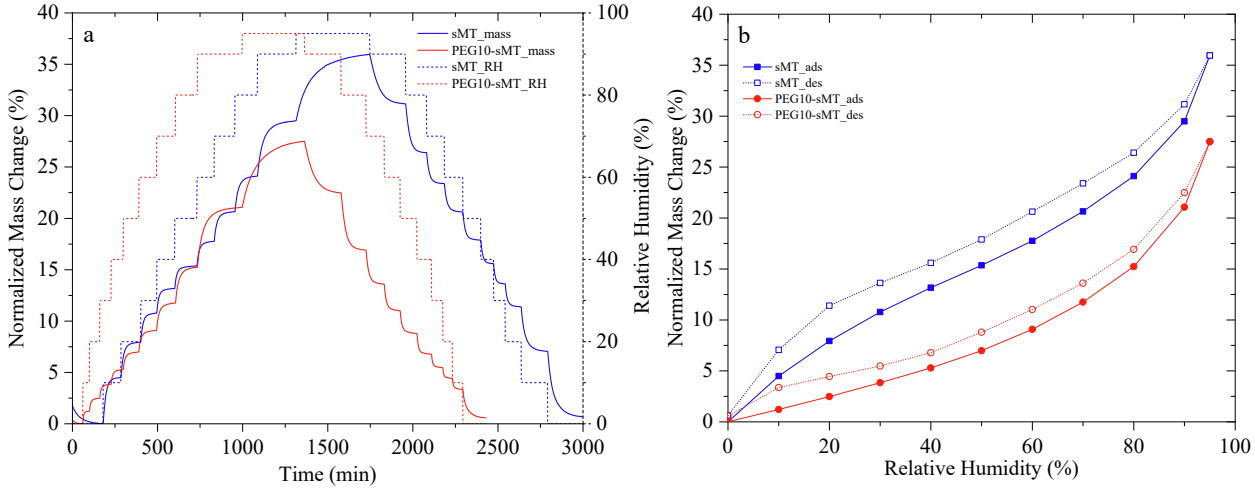

Fig. 4. Dynamic vapor sorption (a) and isotherms (b) of sMT and PEG10-sMT.

[46]: (1) a rapid increase in the moisture adsorption before an inflection point (called the "B" point), which is 20% RH for sMT and 10% RH for PEG10-sMT, indicating a monolayer adsorption period; (2) a moderate increase after the "B" point up to around 90% RH and 80% RH here for sMT and PEG10-sMT respectively, caused by multilayer adsorption; (3) increased moisture adsorption rate without plateau due to capillary condensation. PEG10-sMT exhibits lower values than sMT in both the equilibrium mass and relative hysteresis, indicating that the functionalization can decrease the vapor up-take behavior of sMT during the three segments of the sorption isotherms.

3.1.4. Dispersion in simulated concrete pore solutions

Fig. 5 shows the UV–Vis diffuse absorbance spectra of sMT and PEG10-sMT in simulated pore solution within the 200–1000 nm wavelength range. According to Beer's law, the optical absorbance of the suspension in solution represents the concentration of the substance, as the absorbance is linearly correlated to the corresponding concentration [47]. The untreated sMT particle yields a small peak at 223 nm with an absorbance of 0.06 AU. After the functionalization treatment, the PEG10-sMT shows higher absorbance than the untreated sMT for the entire wavelength range. Different from the untreated sMT, PEG10-sMT shows characteristic absorbance peaks at both 223 nm and 274 nm, where the absorbances were increased by 12 and 18 times, respectively. The increased absorbance peaks indicate the positive role of the functionalization in improving the dispersion of sMT particles in the simulated pore solution [48]. The better dispersion of the functionalized sMT in the simulated concrete pore solution implies a more uniform distribution and less agglomeration in the cement composites, thereby benefiting its pozzolanic reactivity and enhancement of cement hydration.

3.2. Isothermal calorimetry

Fig. 6 shows the heat evolution (heat flow) of the cement blends normalized by the mass fraction of cement, respectively. It should be noted that the surfactant might affect the cement hydration kinetics, and therefore, the isothermal calorimetry results directly [49]. In this study, the non-ionic surfactant, PEG-10, was first intercalated into the interlayer space of sMT before mixing with the cement. From the characterization of the functionalized sMT, it is believed that the isothermal calorimetry results were modified primarily by the functionalized montmorillonite with enhanced physical and chemical properties. The surfactant is considered a part of the functionalized montmorillonite.

The five classic stages could be identified from the heat flow curves of all the 5 groups with varying dosages of either pristine sMT or PEG10-sMT: (1) the initial stage due to the rapid hydration of C_3A in the first minutes after mixing with water; (2) the induction period with a sharply decreased reaction rate; (3) the acceleration period corresponds to the hydration of C_3S that results in the prominent peaks; (4) the deceleration period with reduced reaction rate mainly controlled by the diffusion of ions, where a "post-peak" between 22 and 30 h induced by the transformation of ettringite (AFt) to monosulfate (AFm) can be observed; and (5) the steady-state or diffusion-controlled stage with a very slow hydration rate, which depends on the availability of the spare space for further cement hydration products.

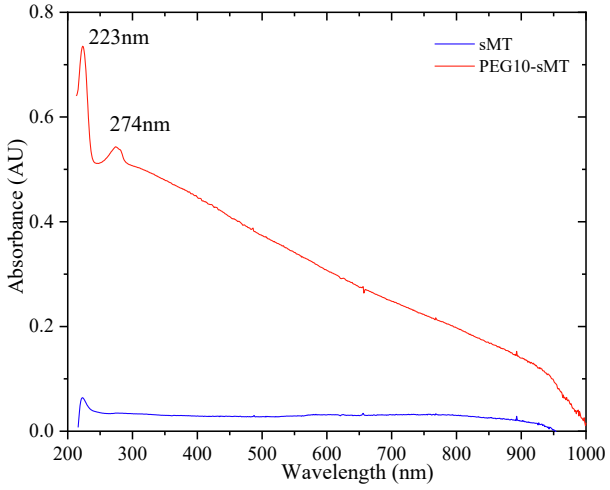

Fig. 5. UV–vis spectra of sMT and PEG10-sMT in a simulated pore solution.

The length of the induction period could be obtained from the normalized heat flow curves using the method proposed by Betioli et al. [50], that the onset and offset points are the intersections of the horizontal baseline of the lowest point with the extrapolations of the sharp decreasing in the initial stage and the increase in the acceleration period, respectively. As shown in Fig. 6b, the induction period could be accelerated and shortened in the presence of sMT. The PC exhibited an induction period in the range of 25.5–178.5 min with a length of 153.0 min. By incorporating 1 wt% and 3 wt% sMT, this "slow reaction" period was decreased to 152.8 and 143.3 min, respectively (see Fig. 6c). This indicates that, in the presence of sMT, the supersaturation of CH and C-S-H in the solution and the nucleation of C-S-H on C_3S surfaces by balancing Ca/Si ration. With the incorporation of functionalized sMT, the induction period was further shortened. The induction periods of PEG10-sMT-1 and PEG10-sMT-3 are 23.0–165.3 min and 21.6–144.8 min with lengths of 142.3 min and 123.2 min, respectively. The earlier onset and shorter "slow reaction" induction period in the presence of the functionalized sMT reveal the modified interlayer space induced by the non-ionic surfactant can enhance the reactive role of this clay mineral in enhancing the cement hydration. This is also evidenced by the increased heat release during the induction period, which is reversely related to the order of the induction period length, i.e., PEG10-sMT-3 > PEG10-sMT-1 > sMT-3 > sMT-1 > PC (see Fig. 6b).

The main differences after the incorporations of sMT and PEG10-sMT in the heat flow curves are observed in the third and fourth stages, namely the acceleration and deceleration periods. As shown in Fig. 6a, earlier start, higher slopes, and increased peak values of the acceleration stage were obtained from the groups containing sMT and PEG10-sMT, indicating the positive roles of sMT and PEG10-sMT nanoparticles in enhancing early age cement hydration and forming C-S-H by providing additional nucleation sites. As reported by Bullard et al. [51], the rate of cement hydration is usually proportional to the number of nuclei sites for C-S-H. It was presented that the peaks corresponding to silicate and secondary aluminate reactions increased with the increasing amount of sMT and PEG10-sMT, indicating that the enhancement of cement hydration is positively correlated with cement substitution level at least in the range of 3 wt%. It is interesting to find that, at the investigated cement substitution levels, PEG10-sMT shows a more significant acceleration effect on cement hydration than the pristine sMT. The peak due to the reaction of C_3S in the group of PEG10-sMT-3 appeared at 7.6 h, which is 0.8 h and 0.6 h earlier than the neat PC and sMT-3, respectively (see Fig. 6d). Even with less cement substitution, the PEG10-sMT-1 shows an earlier and higher exothermic peak than sMT-3. This clearly demonstrates the benefit of non-ionic surfactant functionalization on the pozzolanic reactivity of sMT.

By incorporating sMT or PEG10-sMT, the heat flow peak due to the secondary aluminate reaction was also remarkably increased, especially in the group containing 3 wt% PEG10-sMT. This might be due to the higher aluminate content in the sMT than in the PC (see Table. 1). In addition, the secondary dissolution of C_3A exhibits a strong dependence on the depletion of sulfate-induced by the absorption of sulfate ions by the C-S-H [52] and the formation of ettringite. It was observed that, in the presence of functionalized sMT, sulfate depletion was enhanced and accelerated, which coupled with the increased amount of aluminate in the cement system to trigger the increased secondary reaction of aluminate phases. According to an investigation by Cheung et al. [53],

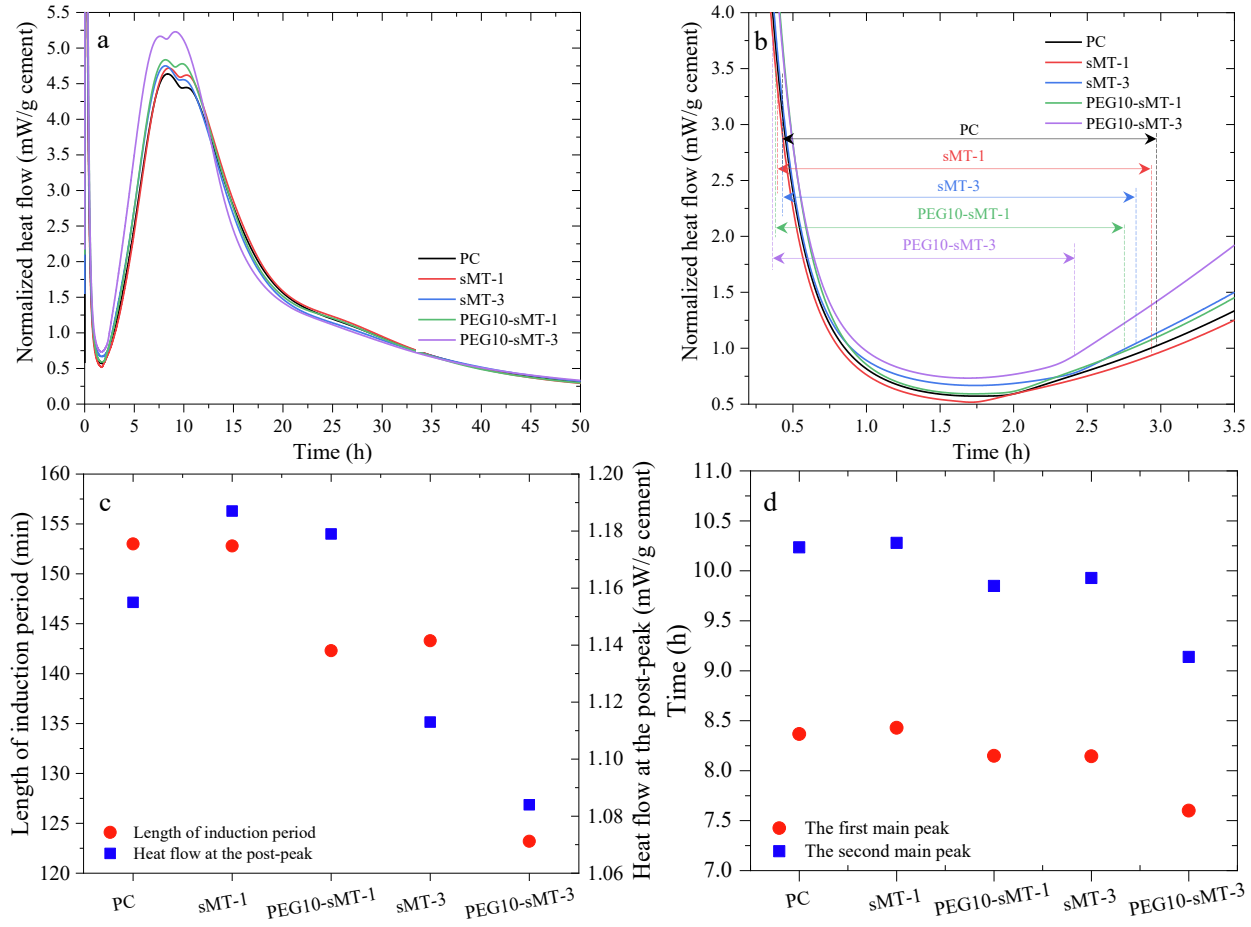

Fig. 6. (a) Normalized specific heat flow and the enlarged views of (b) the induction period, (c) the length of the induction period and heat flow at the "post peak", and (d) the time of the first and second main peaks for the neat cement and cement blends containing sMT and PEG10-sMT at 25 °C.

the formation of ettringite can continue even after sulfate was depleted by using the sulfate released from C-S-H as a sulfate resource. With less sulfate remaining in the C-S-H phases, a lower content of capillary porosity can be obtained [54], thereby resulting in a denser microstructure. From Fig. 6c, the sulfate-depletion peak in the neat PC group appeared at around 10.2 h, while the peaks in the groups with 1% sMT and 3% sMT were at around 10.3 h and 9.9 h, respectively. In the presence of functionalized sMT, this peak was moved earlier to 9.8 h and 9.1 h for PEG10-sMT-1 and PEG10-sMT-3, respectively (see Fig. 6d). Besides, higher peaks were observed from the groups containing sMT with increasing dosage, which is even more significant with the addition of the functionalized PEG10-sMT.

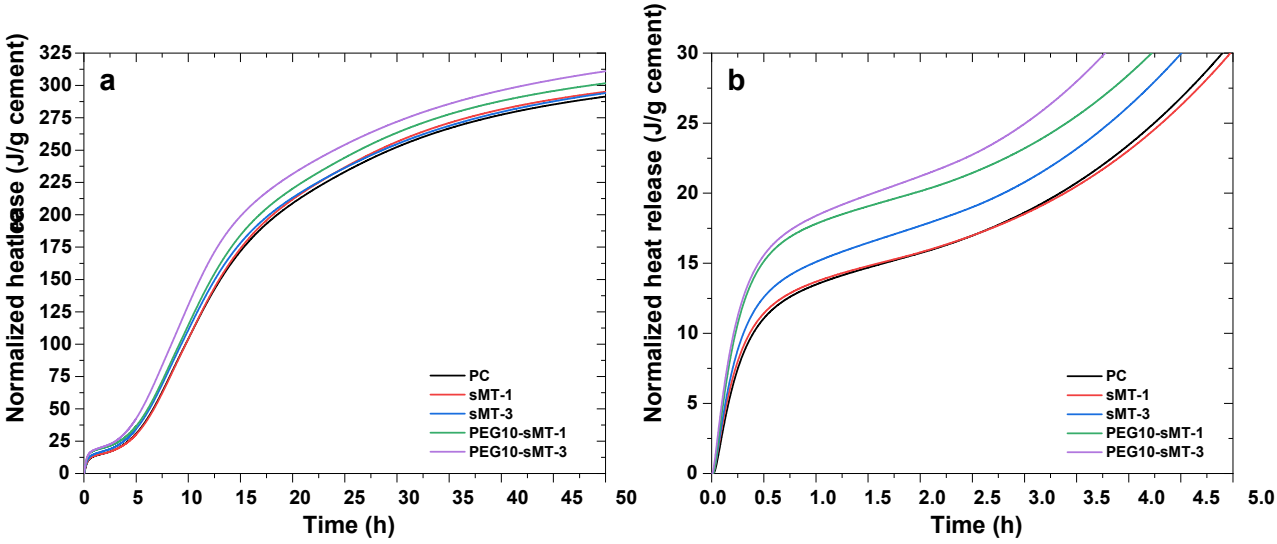

Fig. 7. (a) The cumulative heat release of the cement blends containing sMT and PEG10-sMT at 25 °C and (b) the enlarged view for the first 5 h.

In the deceleration period, the deceleration rate of the reactions was increased by incorporating the raw and functionalized sMT, and PEG10-sMT-3 exhibited the highest deceleration rate. The "post-peaks" of the neat PC, sMT-1, PEG10-sMT-1 were somewhat comparable, indicating no significant influence of low dosage of sMT and PEG10-sMT on the formation of AFm from C_3A and ettringite, as well as the ion diffusion in the cement pastes. However, it can be observed that this peak decreased due to the 3% cement replacement of both the raw and functionalized sMT. This suggests that less mobility of ions in the hydrated cement pastes and less ettringite for the transformation reaction in the presence of high incorporation of sMT. The further reduced heat flow value for the "post peak" from PEG10-sMT-3 confirmed the enhanced role of the functionalized sMT in densifying the microstructure and consuming ettringite of hydrated cement.

The cumulative heat released by the neat and binary cement blends containing varying amounts of sMT and PEG10-sMT normalized by the mass fraction of cement in the blends is shown in Fig. 7a. These curves could be divided into five stages, corresponding to those defined above in the heat flow curves, by four inflection points at around 0.5 h, 3 h (see Fig. 7b), 20 h, and 35 h.

It can be observed that the incorporation of either sMT or PEG10-sMT exhibits increased heat release, which suggests a higher degree of

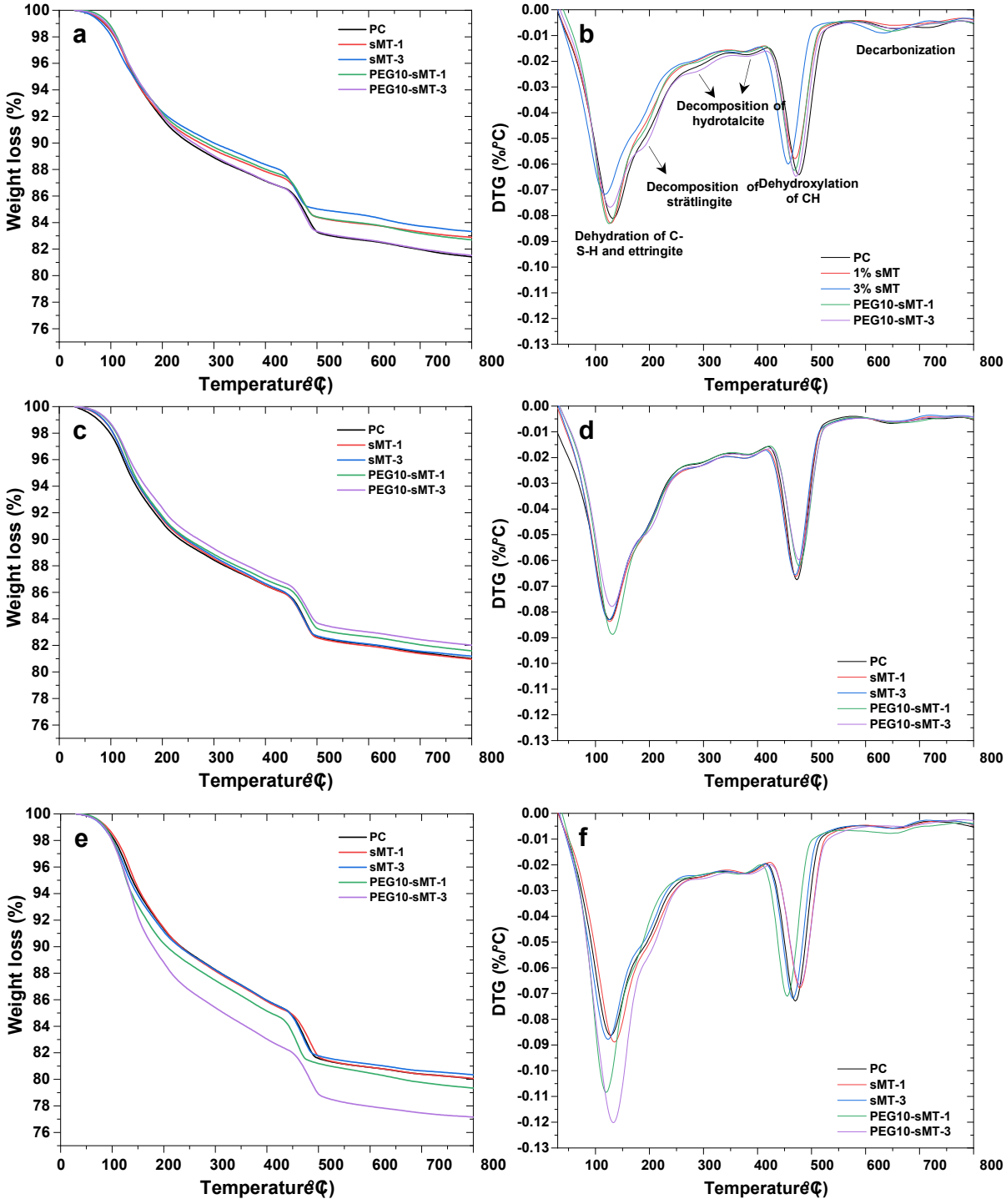

Fig. 8. TGA and DTG curves of neat cement and cement blends containing sMT or PEG10-sMT at (a, b) 7 days, (c, d) 28 days, and (e, f) 90 days.

cement hydration, which was enhanced by the filler and pozzolanic effects of the clay particles [2]. For the pristine sMT, the cumulative heat release was increased with the sMT dosage during the first 24 h, but it reversed in the later testing period up to 50 h, i.e., sMT-1 released more hydration heat than sMT-3, which was probably resulted from the densified microstructure of the cement paste. After 50 h of reaction, the normalized heat release of the neat PC was 291.4 J/g cement, while it increased to 295.1 J/g cement and 294.1 J/g cement in sMT-1 and sMT-3, which are 1.3% and 0.9% higher than that of neat PC, respectively. The slight decrease in heat release of sMT-3 than sMT-1 after 24 h and onward is related to the stable-sate, indicating the role of sMT in enhancing cement hydration is primarily effective during the first 24 h. It is clearly seen that the increase of cumulative heat release was more pronounced in the groups incorporated with the functionalized sMT, which is positively correlated to the dosage of PEG10-sMT. More interestingly, the most pronounced cement hydration enhancement was observed in the cement paste containing 3% PEG10-sMT, especially during the period at around 10–13 h, which was correlated to the mostly enhanced exothermic peaks in Fig. 6a. After 50 h of reaction, the normalized heat release of the PEG10-sMT-1 and PEG10-sMT-3 was 301.7 J/g cement and 311.0 J/g cement, respectively, which was 2.2% and 5.7% higher than that of the blends containing the same dosages of pristine sMT. These observations in further cement hydration enhancement revealed the improved pozzolanic reactivity of sMT triggered by the organic functionalization.

3.3. Thermogravimetric analysis

Thermogravimetric and the corresponding differential thermogravimetric analyses (TGA and DTG) are widely used to quantify cement hydration products based on the mass loss at different temperature ranges. Fig. 8a to 8f present the TGA and DTG curves measured from the neat and binary cement blends containing raw and functionalized sMT after 7 days, 28 days, and 90 days. The main hydration products, such as C-S-H, ettringite, and portlandite (CH), could be identified from the weight drop in the TGA curves and the corresponding peaks in the DTG curves. The initial weight drops in the temperature range from 25 °C to 120 °C show the evaporation of free water in the samples. The overlapped peaks that appeared in the temperature range of 120 to 170 °C are due to the dehydration of C-S-H and ettringite phases. The decomposition of strätlingite was located in the temperature range of 170–250 °C. The following characteristic two-stage peaks at 260–340 °C and 350–400 °C are corresponding to hydrotalcite ($Mg_4Al_2(CO_3)(OH)_{12}{\cdot}4H_2O$), an Mg-Al layered double hydroxide phase. Moreover, the peaks located at 400–510 °C and 590–770 °C are due to the dehydroxylation of CH and the decomposition of CC, respectively.

For the neat PC, it can be seen that the intensity of the peaks due to the decomposition of cement hydrates, i.e., C-S-H and ettringite, was increased over time, which is expected and indicates the increased DOH of cement. Two minor peaks attributed to the decomposition of hydrotalcite, which was formed from the small amount of Mg and Al in the cement and increased with hydration time, were detectable in the control group. Compared with the neat PC, less weight losses due to the decomposition of ettringite and C-S-H were observed from sMT-3 and PEG10-sMT-3 at 7 days. However, an opposite trend at early ages was observed in the cement blends containing 1 wt% sMT and PEG10-sMT. In the later ages (90 days), it can be seen that the overlapped peaks due to the decompositions of C-S-H and ettringite increased significantly in the binary blends, especially for the groups with PEG10-sMT. A new peak due to the decomposition of strätlingite appeared from the binary blends indicating the effective reaction between the aluminate in sMT and cement hydration products. It is interesting to see that PEG10-sMT-3 yielded the highest peak of strätlingite, especially after 90 days, demonstrating the most notable pozzolanic reaction as a result of the functionalization. It is also worth noting that more hydrotalcite, an additional hydration product from the pozzolanic reaction, was observed in the cement blends containing sMT and PEG10-sMT, which might be due to the relatively high content of Al and Mg in sMT. The increased amount of the unique strätlingite and hydrotalcite phases again indicates the enhancement of pozzolanic reactivity of the functionalized sMT.

Agreeing with the previous studies [10,55,56], the role of sMT in cement hydration is a combination of nucleation and pozzolanic reactivity. From the 7-day TGA data (Fig. 8a and 8b) and the first 50 h of calorimetry results (Fig. 7), the enhanced dehydration peak and heat flow peaks, the decreased time of the first and second main peaks, as well as the shortened length of the induction period all indicate the nucleation role of sMT in early-age cement hydration. However, the formations of additional C-S-H, strätlingite, and hydrotalcite phases, as well as the consumption of CH at later ages, reveal the pozzolanic role of sMT, in particular, the one after functionalization.

The CH contents in the neat PC and cement blends calculated from the TGA curves at the three testing ages are presented in Fig. 9a. As expected, the CH content of neat PC increased over time. Less CH was formed in the groups containing sMT and PEG10-sMT, which was mainly due to the CH consumption from the pozzolanic reaction induced by sMT. 13.5% of CH was formed in neat PC after 7 days of hydration, while it decreased to 12.5% and 12.1% in the pastes containing 1% and 3% sMT, respectively, i.e., 7.6% and 10.9% CH was consumed. It should be noted that at 7 days, more CH was obtained from PEG10-sMT-3 than PEG10-sMT-1. This indicates that, at an early age, although there exit pozzolanic reactions, the cement hydration enhancement triggered by the functionalized sMT dominated the change of CH content. At the later ages, more CH was consumed in the PEG10-sMT groups than in the cement blends containing raw sMT. After 90 days of hydration, the neat PC yielded a CH content of 14.5%, while the groups containing 1% and 3% sMT showed 13.6% and 13.3% less CH, respectively. A more pronounced decrease of CH was observed from the groups incorporated with functionalized sMT. At 90 days, the incorporations of PEG10-sMT resulted in 0.7% and 0.6% less CH than the raw sMT at 1% and 3% cement substitutions, respectively. This indicates the higher pozzolanic reactivity of sMT with the functionalization of non-ionic surfactants. A positive correlation between CH consumption and cement replacement level can be obtained, which is in good agreement with the observations from the phase analysis and calorimetry above.

Fig. 9b shows the DOH of cement in the five groups. The DOH of neat PC at 7 days was 43.7%, which increased to 57.5% and 58.9% after 28 days and 90 days, respectively. It shows that the cement hydration is limited even after 90 days of reaction, and it only increased by 1.4% from 28 days to 90 days. By adding 1% and 3% of sMT, the DOHs of cement were increased to 47.3% and 47.9% at 7 days, respectively, which are 8.2% and 9.6% higher than that of neat PC. However, after 90 days, the enhancement effects of sMT on cement hydration decreased to 6.9% for both the cement substitution levels indicating the faded long-term role of the raw sMT. PEG10-sMT-1 showed DOHs of 49.8%, 58.1%, and 64.4% after 7 days, 28 days, and 90 days, which are 13.8%, 10.7%, and 9.3% higher than that of PC, respectively. An extraordinary cement hydration enhancement effect was observed from the group of PEG10-sMT-3, which yielded cement DOHs of 54.8%, 61.1%, and 73.0% after 7 days, 28 days, and 90 days, respectively. From Fig. 9b, it can be seen that an increase in cement replacement from 1% to 3% with raw sMT didn't result in further enhanced DOH of cement. However, a clear positive correlation between cement DOH and its substitution level was observed from the blends containing PEG10-sMT. This again confirmed the benefit of non-ionic functionalization to sMT in enhancing its reactivity and cement hydration.

3.4. X-ray diffraction analysis

In addition to TGA, the influence of the raw and functionalized sMTs on cement hydration products was also evaluated through XRD. Fig. 10 shows the XRD patterns of the cement blends incorporating varying

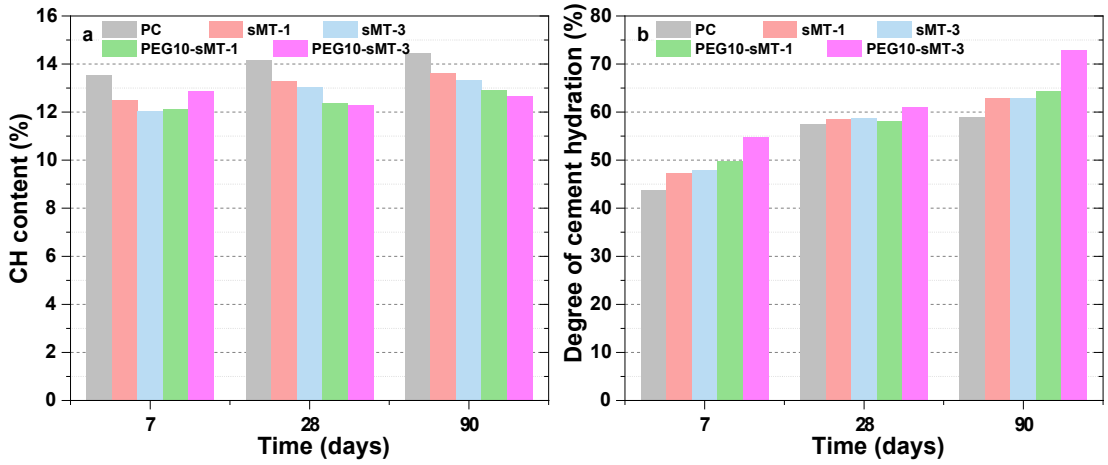

Fig. 9. (a) Calcium hydroxide content and (b) degree of cement hydration determined by TGA.

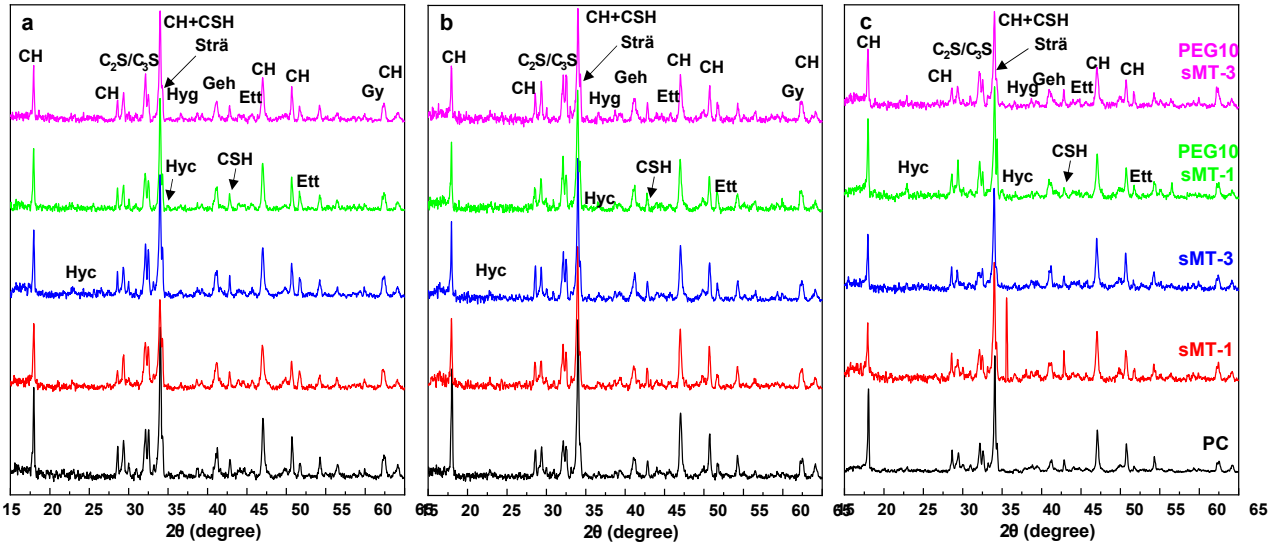

Fig. 10. XRD patterns of cement blends at (a) 7 days, (b) 28 days, and (c) 90 days. CH: calcium hydroxide; Ett: ettringite; Strä: strätlingite; CSH: calcium silicate hydrates, Hyg: hydrogarnet; Hyc: hydrotalcite; Geh: gehlenite; C_2S/C_3S: belite/alite.

amounts of sMT or PEG10-sMT after 7 days, 28 days, and 90 days of reaction, wherein the main hydration products, such as CH, C-S-H, ettringite, hydrogarnet, hydrotalcite, and gehlenite were identified. Besides, non-hydrated minerals, such as C_2S and C_3S, were also detected. The multiple peaks at 18°, 28.5°, 34°, 47°, 50.66°, 54°, and 64.2° 2θ were assigned to CH. The C-S-H phases show a peak at 34° 2θ overlapped with CH, and more C-S-H could be detected at 42.78° 2θ. Moreover, the hydration products, such as strätlingite (C_2ASH_8, at around 34° 2θ), hydrogarnet (C_3AH_6, at around 36.59° 2θ), and hydrotalcite ($Mg_4Al_2(CO_3)(OH)_{12}{\cdot}4H_2O$, at around 22.9° and 33.94° 2θ), were also detected from the cement blends containing sMT and PEG10-sMT resulted from the pozzolanic reaction between CH and Si-/Al-rich phases in sMT as analyzed above.

For the neat PC, the intensity of the CH and C-S-H peaks increased with hydration time, which again revealed the expected increasing DOH of cement. As shown in Fig. 10a, ettringite was formed from an early age, and its amount increased gradually with the simultaneous decrease of gypsum over time (see Fig. 10b and 10c), which is in line with the observation by Sakai et al. [57]. Agreeing well with the TGA curves above, two minor peaks at ~ 22.9° and ~ 33.94° 2θ corresponding to the formation of hydrotalcite were originated from the reaction between magnesium and aluminum in cement also identified from the neat PC during the whole testing period, but no significant change over time was observed.

By incorporating sMT and PEG10-sMT, it can be seen that the evolution of CH in the cement systems was altered. On the one hand, the apparent decreasing trend of CH with the dosage was observed; on the other hand, at each of the given types of clay and dosages, the detected amount of CH decreased with hydration time. It is more than worth noting that the decrease rate of CH after 90 days (see Fig. 10c) was more significant than at the early ages, which is consistent with the TGA results. The higher pozzolanic reactivity of PEG10-sMT than sMT was again observed from the further reduced intensity of CH peaks. Compared with the neat PC, the cement systems with the incorporation of sMT and PEG10-sMT exhibited higher intensity of C-S-H peaks at each age. Moreover, the peaks due to the crystallization of aluminum-containing phases, such as strätlingite and hydrogarnet, also appeared in the groups with sMT and PEG10-sMT. The improved pozzolanic reactivity of sMT triggered by the PEG10 functionalization was also demonstrated by the formation of additional C-S-H and C-A-S-H phases. Although ettringite was observed in these binary blends, especially at an early age, its intensity decreased with time. Examples are the PEG10-sMT groups, which showed the highest intensity for the peaks associated with ettringite at 7 days and the absence of the same phase after 90

days. This is not only due to the enhanced early-age cement hydration in the presence of the sMT functionalized with PEG10, but also the ettringite consumption with a possibility of accelerating its transformation at late ages. Another clear decreasing trend was observed from the peak intensity of the non-hydrated cement clinker minerals (C_2S/C_3S), which not only decreased over time in all groups but also the cement substitution level. For both the two given dosages, PEG10-sMT showed less amount of C_2S/C_3S remained than the PC and sMT groups.

3.5. ATR-FTIR spectroscopy

Fig. 11 displays the ATR-FTIR spectra of the cement blends after 7 days, 28 days, and 90 days of reaction with distinguished characteristic peaks corresponding to cement hydration products. The peaks at ~ 3400 cm^{-1} and ~ 1650 cm^{-1} are caused by the bending vibration of the irregularly bound or absorbed water molecules. It can be seen that the peaks assigned to water molecules become broader with the hydration time, which has also been observed in previous studies [58,59]. Such increased intensity and area of water molecules from the cement pastes over time might imply the stronger bonding between the hydration products and water [58]. It should be noted that the most pronounced water bonding could be observed from the cement paste containing PEG10-sMT, and PC shows the lowest value. The peak at ~ 3640 cm^{-1} is assigned to the O–H stretch mode in CH. The peaks at ~ 954 cm^{-1} and ~ 454 cm^{-1} are associated with the Si-O stretching and bending vibration, which are indicatives of the polymerization of silicate (SiO_4^{2-}) from the C-S-H phase. The minor peak at ~ 820 cm^{-1} is attributed to the asymmetric stretching vibration of Si-O-Si or Si-O-Al bonds, indicating the coexistence of C-S-H and C-A-S-H gels.

Agreeing well with the results from TGA and XRD, the progress of cement hydration in neat PC over time was revealed by the increasing intensity of the CH and C-S-H peaks. On the contrary, time-dependent decreased intensity of CH peaks and the higher C-S-H peaks were detected from the samples containing either sMT or PEG10-sMT. It should be noted that, at both of the cement replacement levels, the decreased intensity of the CH peak and the increased C-S-H peaks were more significant in the case of PEG10-sMT than that of sMT, which again demonstrated the improved pozzolanic reactivity of sMT after functionalization. The broad peak at ~ 645 cm^{-1} is associated with the ettringite's Ca/Al-OH bending mode, and the peak at ~ 1100 cm^{-1} corresponds to the vibration of sulfates (SO_4^{2-}) from ettringite [58]. It can be observed that the ettringite peak from the neat PC group increased with the hydration time. The intensity of the ettringite peak was higher in PEG10-sMT-3 than that of neat PC at 7 days, which is consistent with the observation from the calorimetry studies and indicates the enhanced cement hydration and the less transformation of AFt to AFm in the presence of the functionalized sMT during the early ages. However, contrary to neat PC, decreased ettringite with hydration time was observed from the binary blends containing sMT and PEG10-sMT. After 90 days of reaction, this phase was absent in the groups with 1% and 3% PEG10-sMT. More interestingly, new broad shoulders at around ~ 520 cm^{-1} triggered by strätlingite or calcium aluminosilicate hydrates (C-A-H), the intensity of which increased over time, were obtained from the groups containing sMT and PEG10-sMT.

3.6. Raman spectroscopy

The Raman spectra of the cement pastes after 7 days and 90 days of hydration are depicted in Fig. 12. The peaks at ~ 356 cm^{-1} and the range of 1400 ~ 1700 cm^{-1} related to the stretching vibration of –OH from portlandite (CH) are obtained. The peaks located in the range of 400 ~ 800 cm^{-1} are attributed to the vibration of Si, Al-O-Al, Si bonds, which are assigned to the C-S-H and C-A-S-H phases. The peak identified at ~ 928 cm^{-1} is also caused by the deformation vibration in C-S-H, while the peak at 1079 cm^{-1} is due to the vibration of C-S-H or calcite (CC). The ettringite presents Raman bands at ~ 985 cm^{-1}, and the bands with several signals in the range from 1100 to 1300 cm^{-1} are assigned to the vibration of SO_4^{2-} from different sulfate phases (AFt and AFm). The peak at around ~ 832 cm^{-1} is designated to C_3S and C_2S, while the one at ~ 1345 cm^{-1} is due to the "C–C–C" skeleton, which might be induced by the alcohol used for stopping cement hydration.

From the neat PC, the peaks due to the vibration of CH, ettringite, and C-S-H were increased from 7 days to 90 days, while the reduction of C_2S/C_3S was observed, which follows the cement hydration process. By incorporating sMT into the cement pastes, it can be seen that the CH contents decreased significantly compared to the neat PC at the given age, which is due to the CH consumption from the pozzolanic reaction. sMT-3 even shows a more pronounced CH decreasing than sMT-1, which is reasonable. However, the CH contents kept increasing overtime at the given dosage of sMT, indicating the limited CH consumption capacity of the relatively low dosages of sMT have been incorporated in this study. Besides, more C-S-H and additional C-A-S-H phases could be observed,

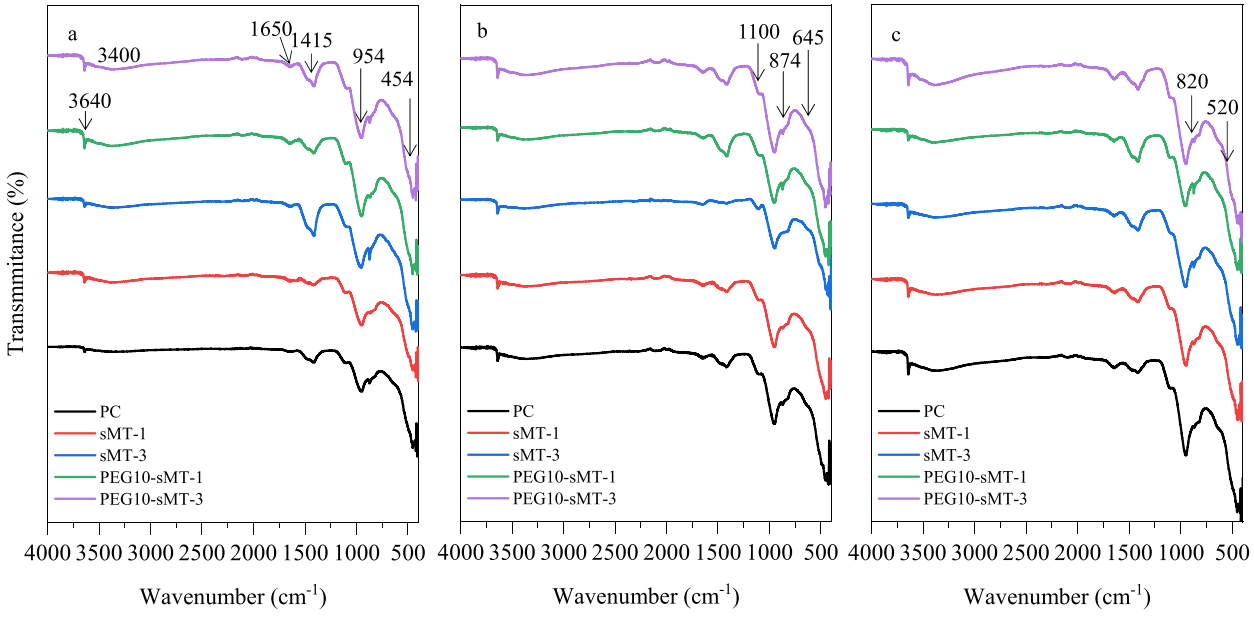

Fig. 11. FT-IR spectra for cement pastes at (a) 7 days, (b) 28 days, and (c) 90 days.

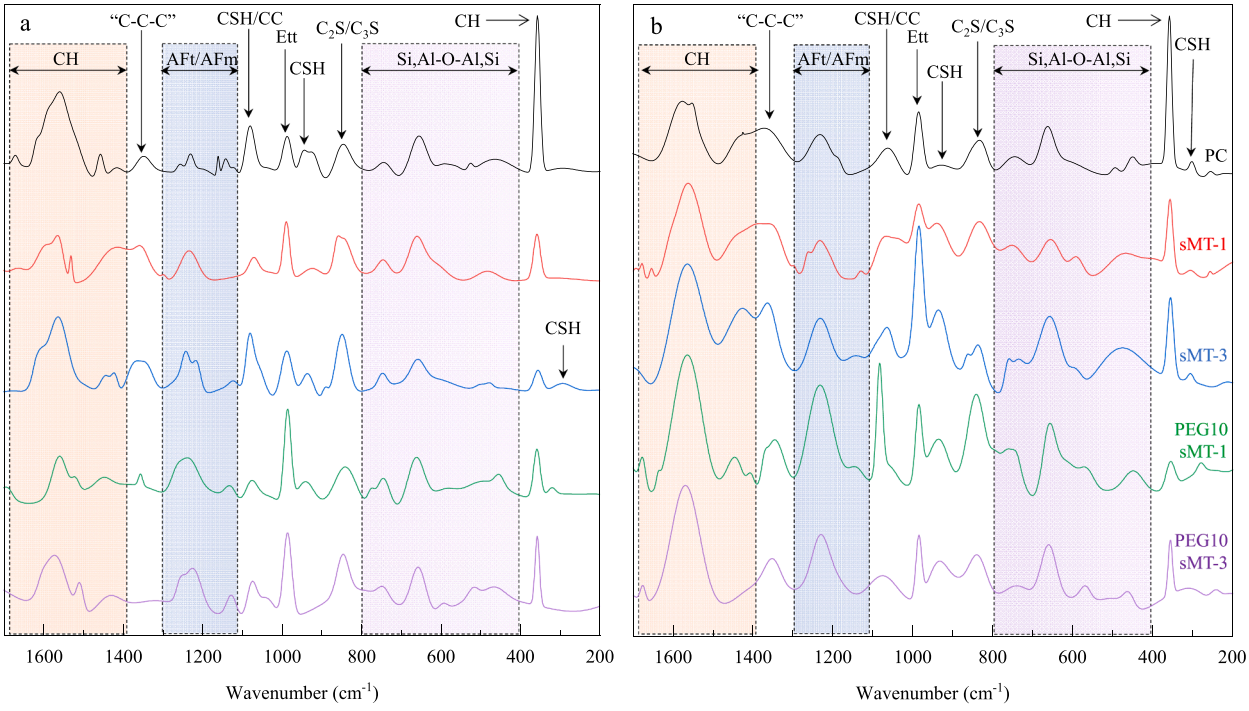

Fig. 12. Raman spectra of cement pastes at (a) 7 days and (b) 90 days.

especially in the group incorporating 3% sMT. Moreover, decreased ettringite was formed in the sMT-1 group compared to the neat PC, but a reversed trend was observed from sMT-3, as more ettringite was identified from its Raman spectra. The same observations, such as less CH, more C-S-H, additional C-A-S-H, compared to the neat PC, were also applied to the groups containing either 1% or 3% of PEG10-sMT. More interestingly, the decreased CH contents from 7 days to 90 days were observed from these two groups, which is consistent with the TGA results, indicating the increased pozzolanic reactivity of the sMT after functionalization.

3.7. Compressive strength

The development of compressive strength of cement mortars with various amounts of sMT and PEG10-sMT clay particles up to 90 days is shown in Fig. 13a. It is seen that the neat PC yielded the highest 1-day compressive strength of 31.2 MPa among all the groups. By incorporating 1% and 3% sMT, the 1-day strength was reduced to 29.5 MPa and 27.7 MPa, respectively. At the same corresponding dosages, the functionalized sMT resulted in a further decrease in 1-days strength, i.e., PEG10-sMT-1 of 28.0 MPa, and PEG10-sMT-3 of 21.6 MPa. From 7 days, the compressive strength of the cement blend containing 1% sMT exhibited a dramatic increase and became 2.3%, 5.1%, and 1.5% higher than the neat PC at 7 days, 28 days, and 90 days, respectively. However, when the dosage of sMT was increased to 3%, lower compressive strength than the neat PC was observed, indicating that 1% might be the optimal dosage of sMT in improving the mechanical strength of cement, which is consistent with the previous studies [21,60]. It is expected that the addition of sMT could improve the strength of mortars mainly due to the filler effect and the pozzolanic reaction. However, the dosage of sMT to play a positive role in improving compressive strength is limited, only 1% here, which might be due to its predominant water absorption capacity and the consequent agglomeration [60] with adverse effects on water distribution and fine clay particles' dispersion in the matrix of

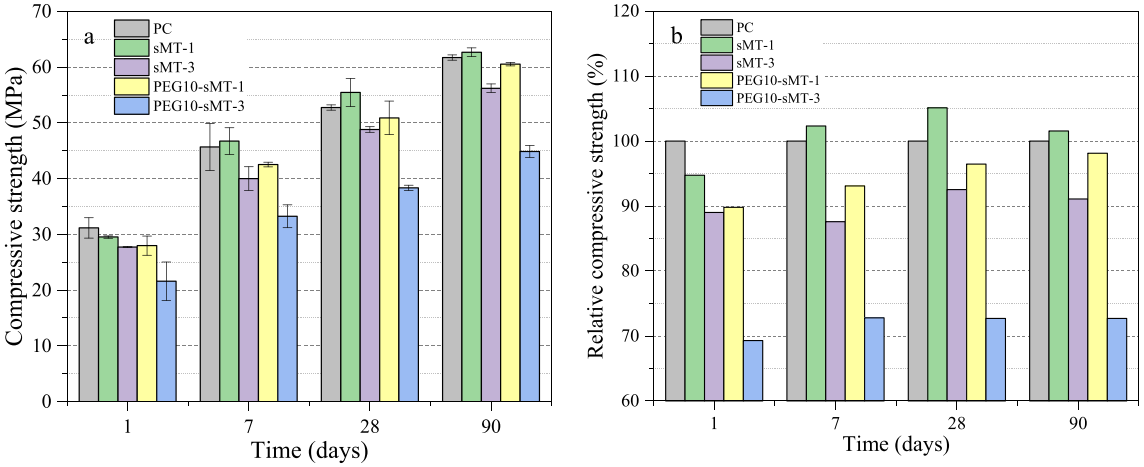

Fig. 13. (a) Compressive strength development and (b) relative compressive strength.

cement.

Although PEG10-sMT shows the higher pozzolanic reactivity and better cement hydration enhancement than the raw sMT as discussed above, its incorporation resulted in lower compressive strength than the neat PC and the cement blends with the same amount of sMT. After 1 day, 7 days, 28 days, and 90 days, PEG10-sMT-1 yielded compressive strength of 28.0 MPa, 42.5 MPa, 50.9 MPa, and 60.5 MPa, which is 10.2%, 6.9%, 3.5%, and 1.9% lower than the neat PC, respectively. Fig. 13b shows the development of the relative compressive strength of the cement blends normalized by the strength of the neat PC group. It can be seen that, from 1 day to 90 days, the relative compressive strength of PEG10-sMT-1 increased from 89.8% to 98.1%. This indicates that the strength loss was probably offset over time by the desired pozzolanic reactivity after functionalization. Similar to raw sMT, a lower strength of blended mortar was observed when the dosage of PEG10-sMT was increased from 1% to 3%. After 1 day, 7 days, 28 days, and 90 days, the relative compressive strength of PEG10-sMT-3 is 69.3%, 72.8%, 72.7%, and 72.7%, respectively. One possibility for the unexpected low compressive strength gained by the PEG10-sMT, especially in the case of 3%, might be the foam produced during mixing caused by the surfactants. The high air content in the mortars negatively impacts the compressive strength development of mortar. In addition, from the author's previous investigation [33], the functionalization with PEG10 can significantly increase the water uptake capacity of sMT, which might also result in less water contribution to fuel cement hydration and more significant particle agglomeration. Therefore, it is recommended to use defoamer (anti-foam agent) or pre-saturated clay particles to trigger internal curing by leveraging the enhanced water absorption capacity when organic functionalized clay particles are used as cement substitutions.

3.8. Microstructure analysis

SEM images of neat PC, sMT-3, and PEG10-sMT-3 after 90 days of reaction are shown in Fig. 14a to 17d. As shown in Fig. 14a and 14b, the main cement hydration products, namely CH, ettringite, and C-S-H phases, are abundant in neat PC. For simple analysis, the microstructure of the target areas of the cement paste was divided into loose and dense zones (see Fig. 14a and 14c). In addition to the typical hexagonal CH sheets and needle-like ettringite crystals that could be observed in the loose zone (left of Fig. 14a), the massive flower-like crystal clusters are composed of rice-shaped grains with an average grain length of 0.3–0.5 μm were observed in the dense zone. According to [61], this phase might be a unique form of CH crystal formed in limited growth space.

By incorporating 3% sMT into cement, fewer ettringite and CH sheets were detected from the loose zone, and the secondary CH crystal clusters with a smaller average size (~0.2 μm) on the surface of C-S-H gels in the dense zone were also observed. On the one hand, the pozzolanic reaction consumed CH and ettringite in the cement pastes to form additional C-S-H and densified microstructure. On the other hand, the addition of sMT may promote the transformation of AFt to AFm, especially in the long-term period. In addition to the cement hydration products, unreacted sMT clay particles were also observed from sMT-3 (Fig. 14c). After functionalizing sMT with 0.2PEG10, as shown in Fig. 14d, different topographical features were observed from the hydrated cement. First, a denser microstructure than the paste of sMT-3 was presented. Second, no needle-like ettringite or CH, either in hexagonal sheet or crystal cluster shape, can be observed, which revealed the enhanced pozzolanic reactivity of sMT triggered by functionalization and the possible acceleration in the transformation of AFt to AFm, which is consistent with the results from TGA, XRD, and ATR-FTIR studies above. These

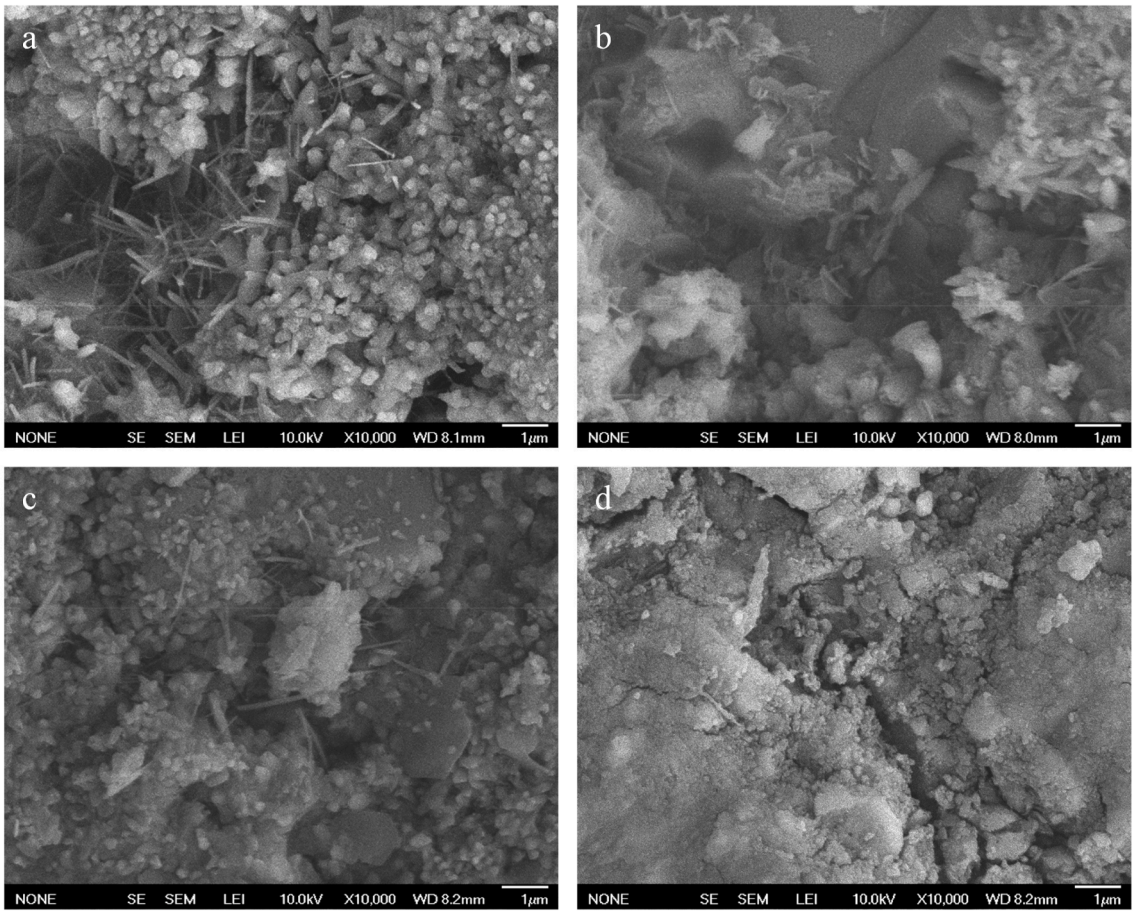

Fig. 14. SEM images of the cement blends cured in saturated lime water at room temperature after 90 days: (a) and (b) PC, (c) sMT-3, and (d) PEG10-sMT-3.

microstructural observations confirmed the great potential of non-ionic functionalization in improving the cement modification efficiency of sMT and its reactivity in cement systems.

4. Conclusions

The effect of sMT and its organic functionalization with a non-ionic surfactant (PEG10-sMT) on hydration kinetics and behavior of cement, as well as its influence on the evolutions of microstructure and mechanical strength, were investigated in this study by means of isothermal calorimetry, TGA, XRD, ATR-FTIR, SEM and strength testing. The experimental observations agree well with each other and demonstrated that the functionalization of sMT can further enhance cement hydration by improving the pozzolanic reactivity of sMT. In summary, the main conclusions of this study include:

(1) PEG10 could be intercalated into sMT to increase the interlayer space. As a result, after functionalization with PEG10, less moisture vapor could be absorbed, while the water absorption capacity of sMT at SSD condition was increased by two times.
(2) The acceleration and enhancement of cement hydration by incorporating sMT and PEG10-sMT were found by the calorimetry analyses, and 3% of PEG10-sMT shows the most remarkable enhancement in cement hydration heat. The induction time was shortened by incorporating 3% sMT, while it decreased more pronounced when PEG10-sMT was incorporated. Accompanying with this is the early occurrence of the first and second main peaks of the normalized heat flow and the increased heat release.
(3) Decreased CH contents were obtained in the presence of sMT and PEG10-sMT with a higher degree of cement hydration. The experimental results from TGA, XRD, ATR-FTIR, and Raman spectroscopy analyses suggest that, compared with neat PC, more C-S-H and additional aluminum-containing phases, such as strätlingite, hydrotalcite, hydrogarnet, and C-A-S-H were formed in the groups containing sMT. With the incorporation of functionalized sMT (PEG10-sMT), the increases of C-S-H and aluminum-containing phases are more significant, indicating the enhanced pozzolanic reactivity of sMT in the presence of the non-ionic surfactant.
(4) By incorporating 1% sMT, the degree of cement hydration was increased by 6.9% after 90 days of hydration. By increasing the dosage of sMT from 1% to 3%, no significant increase in cement DOH was observed, while the cement hydration degree was increased by 23.9% with the incorporation of 3% PEG10-sMT, indicating the extraordinary cement hydration enhancement effect of the functionalized sMT.
(5) In neat PC and sMT-3, the hexagonal portlandite sheets were found in the loose zone, while crystal clusters composed of rice-shaped grains with an average grain length of 0.3–0.5 μm were observed in the dense zone. Denser microstructures were obtained from the cement by incorporating 3% PEG10-sMT with less detectable portlandite and ettringite phases. This is considered as a result of the enhanced pozzolanic reaction and the accelerated transformation of ettringite triggered by the functionalized sMT in cement hydration.
(6) The compressive strength results revealed that the optimal dosage of sMT in improving the compressive strength of cement mortars is 1% by weight. The incorporation of PEG10-sMT caused decreased compressive strength, which might be due to the improved water absorption of the clay particles and the foam formed during mixing in the presence of non-ionic surfactant (PEG10). However, a significant strength gain rate was obtained, and hence a rapid increase of the relative strength over time was observed. Anti-foam agents or pre-saturation of the functionalized clay particles are recommended in future works.

Declaration of Competing Interest

The authors declare that they have no known competing financial interests or personal relationships that could have appeared to influence the work reported in this paper.

Acknowledgment

This work was supported by the United States National Science Foundation (NSF) under the award No. 1935799. The authors gratefully acknowledge the support from this funding.

References

[1] O. Heinz, H. Heinz, Cement Interfaces: Current Understanding, Challenges, and Opportunities, Langmuir (2021), https://doi.org/10.1021/acs.langmuir.1c00617.
[2] J. Wei, B. Gencturk, Hydration of ternary Portland cement blends containing metakaolin and sodium bentonite, Cem. Concr. Res. 123 (2019), 105772, https://doi.org/10.1016/j.cemconres.2019.05.017.
[3] G.L. Golewski, Energy savings associated with the use of fly ash and nanoadditives in the cement composition, Energies 13 (9) (2020) 2184, https://doi.org/10.3390/en13092184.
[4] R.A. Rivera, M.Á. Sanjuán, D.A. Martín, Granulated blast-furnace slag and coal fly ash ternary portland cements optimization, Sustainability 12 (14) (2020) 5783, https://doi.org/10.3390/su12145783.
[5] H. Campos, N. Klein, J. Marques Filho, M. Bianchini, Low-cement high-strength concrete with partial replacement of Portland cement with stone powder and silica fume designed by particle packing optimization, J. Clean. Prod. 261 (2020) 121228. 10.1016/j.jclepro.2020.121228.
[6] M. Nodehi, V.M. Taghvaee, Sustainable concrete for circular economy: a review on use of waste glass, Glass Structures & Engineering (2021) 1–20, https://doi.org/10.1007/s40940-021-00155-9.
[7] S. Ng, J. Plank, Interaction mechanisms between Na montmorillonite clay and MPEG-based polycarboxylate superplasticizers, Cem. Concr. Res. 42 (6) (2012) 847–854, https://doi.org/10.1016/j.cemconres.2012.03.005.
[8] M.L. Whittaker, L.N. Lammers, S. Carrero, B. Gilbert, J.F. Banfield, Ion exchange selectivity in clay is controlled by nanoscale chemical–mechanical coupling, Proceedings of the National Academy of Sciences 116 (44) (2019) 22052–22057, https://doi.org/10.1073/pnas.1908086116.
[9] J. Jiang, Z. Lu, J. Li, Y. Xie, K. Luo, Y. Niu, Preparation and properties of nanopore-rich lightweight cement paste based on swelled bentonite, Constr. Build. Mater. 199 (2019) 72–81, https://doi.org/10.1016/j.conbuildmat.2018.11.278.
[10] R. Fernandez, F. Martirena, K.L. Scrivener, The origin of the pozzolanic activity of calcined clay minerals: A comparison between kaolinite, illite and montmorillonite, Cem. Concr. Res. 41 (1) (2011) 113–122, https://doi.org/10.1016/j.cemconres.2010.09.013.
[11] J. Wei, B. Gencturk, A. Jain, M. Hanifehzadeh, Mitigating alkali-silica reaction induced concrete degradation through cement substitution by metakaolin and bentonite, Appl. Clay Sci. 182 (2019), 105257, https://doi.org/10.1016/j.clay.2019.105257.
[12] N. Mesboua, K. Benyounes, A. Benmounah, Study of the impact of bentonite on the physico-mechanical and flow properties of cement grout, Cogent Eng. 5 (1) (2018) 1446252, https://doi.org/10.1080/23311916.2018.1446252.
[13] S.Y. Kwon, S.S. Kim, Preparation and characterization of bone cements incorporated with montmorillonite, Macromolecular Symposia, Wiley Online, Library 249-250 (1) (2007) 86–95.
[14] S. Papatzani, Effect of nanosilica and montmorillonite nanoclay particles on cement hydration and microstructure, Mater. Sci. Technol. 32 (2) (2016) 138–153, https://doi.org/10.1179/1743284715Y.0000000067.
[15] Y. Xie, J. Li, Z. Lu, J. Jiang, Y. Niu, Effects of bentonite slurry on air-void structure and properties of foamed concrete, Constr. Build. Mater. 179 (2018) 207–219, https://doi.org/10.1016/j.conbuildmat.2018.05.226.
[16] D. Zhou, F. Ji, Study on Energy-Storing Building Materials Made of Paraffin/Montmorillonite Composites, 8th Annual International Conference on Material Science and Engineering (ICMSE2020), J. Phys.: Conf. Ser. 1637 (1) (2020) 012084.
[17] F. Bompadre, C. Scheffler, T. Utech, J. Donnini, Polymeric Coatings for AR-Glass Fibers in Cement-Based Matrices: Effect of Nanoclay on the Fiber-Matrix Interaction, Appl. Sci. 11 (12) (2021) 5484, https://doi.org/10.3390/app11125484.
[18] J.-A. Oh, Y. Zhuge, S. Araby, R. Wang, H. Yu, W. Fan, M. Liu, S.-H. Lee, M.J. Alam, J. Ma, Cement nanocomposites containing montmorillonite nanosheets modified with surfactants of various chain lengths, Cem. Concr. Compos. 116 (2021), 103894, https://doi.org/10.1016/j.cemconcomp.2020.103894.
[19] R. Kalpokaitė-Dičkuvienė, I. Lukošiūtė, J. Čėsnienė, K. Brinkienė, A. Baltušnikas, Cement substitution by organoclay–the role of organoclay type, Cem. Concr. Compos. 62 (2015) 90–96, https://doi.org/10.1016/j.cemconcomp.2015.04.021.
[20] S. Zhu, H. Peng, J. Chen, H. Li, Y. Cao, Y. Yang, Z. Feng, Intercalation behavior of poly (ethylene glycol) in organically modified montmorillonite, Appl. Surf. Sci. 276 (2013) 502–511, https://doi.org/10.1016/j.apsusc.2013.03.123.
[21] P. Yu, Z. Wang, P. Lai, P. Zhang, J. Wang, Evaluation of mechanic damping properties of montmorillonite/organo-modified montmorillonite-reinforced

cement paste, Constr. Build. Mater. 203 (2019) 356–365, https://doi.org/10.1016/j.conbuildmat.2019.01.110.
[22] J.L. Alves, P.d.T.V.e. Rosa, A.R. Morales, A comparative study of different routes for the modification of montmorillonite with ammonium and phosphonium salts, Appl. Clay Sci. 132-133 (2016) 475–484.
[23] L. Zhou, H. Chen, X. Jiang, F. Lu, Y. Zhou, W. Yin, X. Ji, Modification of montmorillonite surfaces using a novel class of cationic gemini surfactants, J. Colloid Interface Sci. 332 (1) (2009) 16–21, https://doi.org/10.1016/j.jcis.2008.12.051.
[24] W.-Y. Kuo, J.-S. Huang, C.-H. Lin, Effects of organo-modified montmorillonite on strengths and permeability of cement mortars, Cem. Concr. Res. 36 (5) (2006) 886–895, https://doi.org/10.1016/j.cemconres.2005.11.013.
[25] L. Morjène, F. Aloulou, M. Seffen, Effect of organoclay and wood fiber inclusion on the mechanical properties and thermal conductivity of cement-based mortars, Comptes Rendus. Chimie 23 (11–12) (2020) 733–746, https://doi.org/10.5802/crchim.42.
[26] S. Papatzani, S. Grammatikos, K. Paine, Permeable nanomontmorillonite and fibre reinforced cementitious binders, Materials 12 (19) (2019) 3245, https://doi.org/10.3390/ma12193245.
[27] G. Wang, S. Wang, Z. Sun, S. Zheng, Y. Xi, Structures of nonionic surfactant modified montmorillonites and their enhanced adsorption capacities towards a cationic organic dye, Appl. Clay Sci. 148 (2017) 1–10, https://doi.org/10.1016/j.clay.2017.08.001.
[28] R. Guégan, Intercalation of a nonionic surfactant (C10E3) bilayer into a Na-montmorillonite clay, Langmuir 26 (24) (2010) 19175–19180, https://doi.org/10.1021/la1039267.
[29] S. Papatzani, K. Paine, Inorganic and organomodified nano-montmorillonite dispersions for use as supplementary cementitious materials–a novel theory based on nanostructural studies, Nanocomposites 3 (1) (2017) 2–19, https://doi.org/10.1080/20550324.2017.1315210.
[30] ASTMC150/C150M, Standard Specification for Portland Cement, 2021, doi: 10.1520/C0150_C0150M-21.
[31] ASTM C837. Standard test method for methylene blue index of clay, ASTM, 2019, https://doi.org/10.1520/C0837-09R19.
[32] K. Taleb, I. Pillin, Y. Grohens, S. Saidi-Besbes, Gemini surfactant modified clays: Effect of surfactant loading and spacer length, Appl. Clay Sci. 161 (2018) 48–56, https://doi.org/10.1016/j.clay.2018.03.015.
[33] D. Luo, J. Wei, Functionalization of montmorillonite with non-ionic surfactants and its potential for internal curing in cement systems (Unpublished results).
[34] T.-P. Chang, J.-Y. Shih, K.-M. Yang, T.-C. Hsiao, Material properties of Portland cement paste with nano-montmorillonite, J. Mater. Sci. 42 (17) (2007) 7478–7487, https://doi.org/10.1007/s10853-006-1462-0.
[35] M. Chen, B. Liu, L. Li, L. Cao, Y. Huang, S. Wang, P. Zhao, L. Lu, X. Cheng, Rheological parameters, thixotropy and creep of 3D-printed calcium sulfoaluminate cement composites modified by bentonite, Composites Part B 186 (2020), 107821, https://doi.org/10.1016/j.compositesb.2020.107821.
[36] ASTM C109/109 M, Standard Test Method for Compressive Strength of Hydraulic Cement Mortars (Using 2-in. or [50-mm] Cube Specimens) (2021), https://doi.org/10.1520/C0109_C0109M-21.
[37] T. Kim, J. Olek, Effects of sample preparation and interpretation of thermogravimetric curves on calcium hydroxide in hydrated pastes and mortars, Transp. Res. Rec. 2290 (1) (2012) 10–18, https://doi.org/10.3141/2290-02.
[38] W. Deboucha, N. Leklou, A. Khelidj, M.N. Oudjit, Hydration development of mineral additives blended cement using thermogravimetric analysis (TGA): Methodology of calculating the degree of hydration, Constr. Build. Mater. 146 (2017) 687–701, https://doi.org/10.1016/j.conbuildmat.2017.04.132.
[39] J.I. Bhatty, Hydration versus strength in a portland cement developed from domestic mineral wastes—A comparative study, Thermochim. Acta 106 (1986) 93–103, https://doi.org/10.1016/0040-6031(86)85120-6.
[40] T.C. Powers, T.L. Brownyard, Studies of the physical properties of hardened Portland cement paste, J. Proc. (1946) 101–132.
[41] J. Tikkanen, A. Cwirzen, V. Penttala, Effects of mineral powders on hydration process and hydration products in normal strength concrete, Constr. Build. Mater. 72 (2014) 7–14, https://doi.org/10.1016/j.conbuildmat.2014.08.066.
[42] S. Gražulis, D. Chateigner, R.T. Downs, A. Yokochi, M. Quirós, L. Lutterotti, E. Manakova, J. Butkus, P. Moeck, A. Le Bail, Crystallography Open Database–an open-access collection of crystal structures, J. Appl. Crystallogr. 42 (4) (2009) 726–729, https://doi.org/10.1107/S0021889809016690.
[43] C.G. Pope, X-ray diffraction and the Bragg equation, J. Chem. Educ. 74 (1) (1997) 129, https://doi.org/10.1021/ed074p129.
[44] B. Lothenbach, Thermodynamic equilibrium calculations in cementitious systems, Mater. Struct. 43 (10) (2010) 1413–1433, https://doi.org/10.1617/s11527-010-9592-x.
[45] K. Sing, D. Everett, R. Haul, L. Moscou, R. Pierotti, J. Rouquerol, Siemieniewska Pure Appl, Chem 57 (1985) 603.
[46] G. Sang, S. Liu, D. Elsworth, Water vapor sorption properties of Illinois shales under dynamic water vapor conditions: experimentation and modeling, Water Resour. Res. 55 (8) (2019) 7212–7228, https://doi.org/10.1029/2019WR024992.
[47] T.G. Mayerhöfer, J. Popp, Beer's Law-Why Absorbance Depends (Almost) Linearly on Concentration, ChemPhysChem 20 (4) (2019) 511–515, https://doi.org/10.1002/cphc.201801073.
[48] J. Alin, M. Rubino, R. Auras, Effect of the Solvent on the Size of Clay Nanoparticles in Solution as Determined Using an Ultraviolet-Visible (UV-Vis) Spectroscopy Methodology, Appl. Spectrosc. 69 (6) (2015) 671–678, https://doi.org/10.1366/14-07704.
[49] A.J. MacLeod, F.G. Collins, W. Duan, Effects of carbon nanotubes on the early-age hydration kinetics of Portland cement using isothermal calorimetry, Cem. Concr. Compos. 119 (2021), 103994, https://doi.org/10.1016/j.cemconcomp.2021.103994.
[50] A. Betioli, P. Gleize, D. Silva, V. John, R. Pileggi, Effect of HMEC on the consolidation of cement pastes: isothermal calorimetry versus oscillatory rheometry, Cem. Concr. Res. 39 (5) (2009) 440–445, https://doi.org/10.1016/j.cemconres.2009.02.002.
[51] J.W. Bullard, H.M. Jennings, R.A. Livingston, A. Nonat, G.W. Scherer, J. S. Schweitzer, K.L. Scrivener, J.J. Thomas, Mechanisms of Cement hydration, Cem. Concr. Res. 41 (12) (2011) 1208–1223, https://doi.org/10.1016/j.cemconres.2010.09.011.
[52] K. Scrivener, A. Ouzia, P. Juilland, A.K. Mohamed, Advances in understanding cement hydration mechanisms, Cem. Concr. Res. 124 (2019), 105823, https://doi.org/10.1016/j.cemconres.2019.105823.
[53] J. Cheung, A. Jeknavorian, L. Roberts, D. Silva, Impact of admixtures on the hydration kinetics of Portland cement, Cem. Concr. Res. 41 (12) (2011) 1289–1309, https://doi.org/10.1016/j.cemconres.2011.03.005.
[54] E.M. Bérodier, A.C. Muller, K.L. Scrivener, Effect of sulfate on CSH at early age, Cem. Concr. Res. 138 (2020), 106248, https://doi.org/10.1016/j.cemconres.2020.106248.
[55] S. Papatzani, E.G. Badogiannis, K. Paine, The pozzolanic properties of inorganic and organomodified nano-montmorillonite dispersions, Constr. Build. Mater. 167 (2018) 299–316, https://doi.org/10.1016/j.conbuildmat.2018.01.123.
[56] S. Khandelwal, K.Y. Rhee, Evaluation of pozzolanic activity, heterogeneous nucleation, and microstructure of cement composites with modified bentonite clays, Constr. Build. Mater. 323 (2022), 126617, https://doi.org/10.1016/j.conbuildmat.2022.126617.
[57] E. Sakai, Y. Nikaido, T. Itoh, M. Daimon, Ettringite formation and microstructure of rapid hardening cement, Cem. Concr. Res. 34 (9) (2004) 1669–1673, https://doi.org/10.1016/j.cemconres.2004.04.021.
[58] M. Mollah, W. Yu, R. Schennach, D.L. Cocke, A Fourier transform infrared spectroscopic investigation of the early hydration of Portland cement and the influence of sodium lignosulfonate, Cem. Concr. Res. 30 (2) (2000) 267–273, https://doi.org/10.1016/S0008-8846(99)00243-4.
[59] I.G. Lodeiro, D.E. Macphee, A. Palomo, A. Fernández-Jiménez, Effect of alkalis on fresh C–S–H gels. FTIR analysis, Cem. Concr. Res. 39 (3) (2009) 147–153, https://doi.org/10.1016/j.cemconres.2009.01.003.
[60] M. Chi, R. Huang, Effect of montmorillonite as additive on the properties of cement-based composites, Science and Engineering of Composite Materials 19 (1) (2012) 45–54, https://doi.org/10.1515/secm-2011-0129.
[61] Y. Wang, J. Yang, D. Ouyang, Effect of graphene oxide on mechanical properties of cement mortar and its strengthening mechanism, Materials 12 (22) (2019) 3753, https://doi.org/10.3390/ma12223753.